Section B, Vol. 9 No. 1

APPLIED SCIENTIFIC RESEARCH

B. ELECTROPHYSICS, ACOUSTICS, OPTICS, MATHEMATICAL METHODS

Reports published under the auspices of

The Central National Organization for Applied Scientific Research in the Netherlands (T.N.O.)

The Netherlands Physical Society, Section for Applied Physics

The Royal Institute of Engineers of the Netherlands, Section for Technical Scientific Research

The Mathematical Centre, Amsterdam

Contents:

THE HAGUE
MARTINUS NIJHOFF
1961

b) Resistive heating of the field-emission centres on the cathode leads to a rupture of one or more of these projections [3–7]).

c) Positive ions, produced at the anode by field-emission electrons, locally heat the cathode [7])[8]).

d) Loosely attached pieces of material (clumps) on either electrode, carrying a charge, are torn from the electrode surface and cross the gap under influence of the field. On striking the other electrode they may cause high temperatures and local evaporation [9]).

e) Breakdown occurs, when at a certain voltage a free electron produces an avalanche of charged particles. Primary electrons may

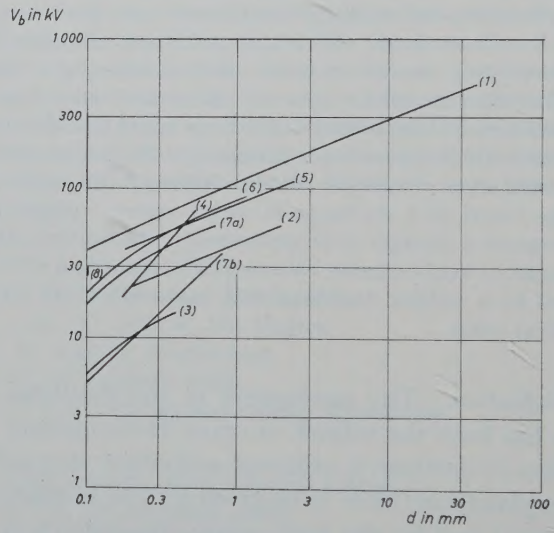

Fig. 1. Breakdown voltage V_b as a function of gap length d.

1. Trump, J. G. and R. J. Van de Graaff, [12]), iron electrodes, impulse voltage.
2. Mason, R. C. [15]), tungsten cathode, copper anode, direct voltage.
3. Leader, D. [16]), iron electrodes ,direct voltage.
4. Rosanova, N. B. and V. L. Granovskii [17]), nickel cathode, molybdenum anode, impulse voltage.
5. Rosanova, N. B. and V. L. Granovskii [17]), molybdenum electrodes, alternating voltage.
6. Denholm, A. S. [7]), iron electrodes, alternating voltage.
7. Wijker, W. J., *a*) iron electrodes, *b*) copper electrodes, alternating voltage.
8. Wijker, W. J., stainless steel electrodes, impulse voltage (d = 0.1 mm only).

produce positive ions and eventually photons at the anode; these, in their turn, striking the cathode, may produce electrons and so the process continues [10–13]).

Because of the great number of variables in the problem, no theory up to now describes quantitatively all experimental results.

Some measurements of the breakdown voltage as a function of gap width are represented in fig. 1. The slope of the curves varies between 0.5 (as predicted by Cranberg's theory [9])) and 1. The voltage gradient in the gap decreases from about 2 MV/cm at a gap width of 0.1 mm to about 60 kV/cm at 10 cm. The spread in the measurements may be caused by differences in degassing methods, in the material and in the shape of the electrodes, as well as in the electrical circuits used (direct, alternating and impulse voltage circuits).

In most previous investigations less attention has been given to the pre-breakdown phenomena. It is to be expected, however, that the pre-breakdown current in the gap is important for the final breakdown. Measurements of this current will be described in this article, both for impulse voltage and for 50 Hz alternating voltage breakdown. § 2 deals with the experimental arrangement. The conditioning of the electrodes will be described in § 3. The results of the measurements are dealt with in the §§ 4 and 5, while in § 6 a discussion of the results is given.

§ 2. *Experimental arrangement.* The experiments have been carried out in two different vacuum chambers, one being a demountable, rubber-sealed vessel, evacuated by a mercury diffusion pump, the other being an all-glass system, directly sealed to an oil diffusion pump. In both cases a liquid-air trap was placed between the pump and the vacuum chamber. With the available pumps a working pressure of 6×10^{-5} and 8×10^{-6} mm Hg respectively could be established. This corresponds to a mean free path of at least 80 cm for molecules (air) and 500 cm for electrons, which is large compared with the dimensions of the gap.

In the demountable apparatus, the distance between the electrodes could be varied during the experiments by means of a rubber membrane, while in the all-glass system this was done by means of an external magnet. Figs. 2 and 3 give cross-sectional views of the vessels. The electrodes in each vessel were of a similar shape and

replaceable. The diameter of the electrodes in the demountable apparatus was 26 mm and the convex surfaces had a radius of curvature of 40 mm. For the all-glass system these figures were 18 and 25 mm respectively. Copper, iron and stainless steel electrodes were used.

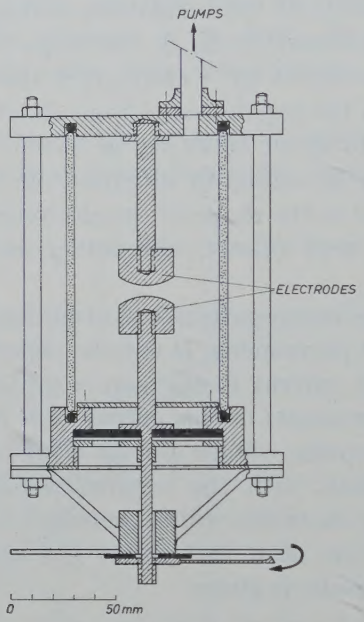

Fig. 2. Cross-sectional view of the demountable vacuum chamber.

The applied tension was either a 50 Hz alternating voltage, adjustable from 0 to 45 kV peak value, or an impulse voltage with a peak value of about 32 kV and a rise time varying from 1.0 μs tot 1.3 ms. In the a.c. circuit a current limiting resistor was placed in series with the gap. The gap voltage was measured with a resistive voltage divider in parallel with the gap. The current was recorded with the aid of a 1000 Ω resistive element.

The impulse voltage was generated by charging a 120 pF condensor through a rise-time defining resistor of variable value (R_t, fig. 4). The charging of this condensor was started by triggering the spark gap SG I, which is initiated by the discharge of a condensor (2 μF) through a thyratron (EC 50) and the primary of an induction coil. This caused the small spark gap SG II to fire. The middle sphere of SG I then fell to earth potential and SG I broke down.

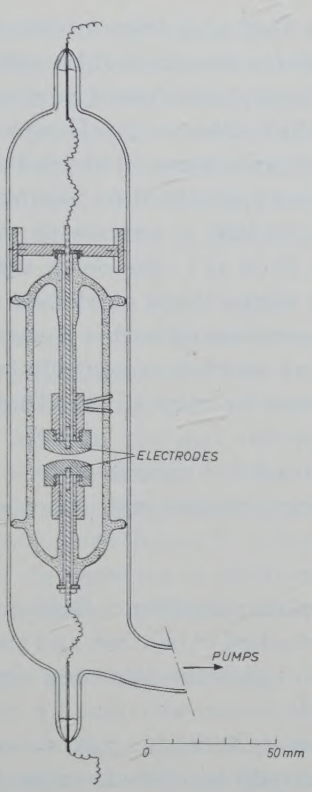

Fig. 3. Cross-sectional view of the all-glass vacuum chamber.

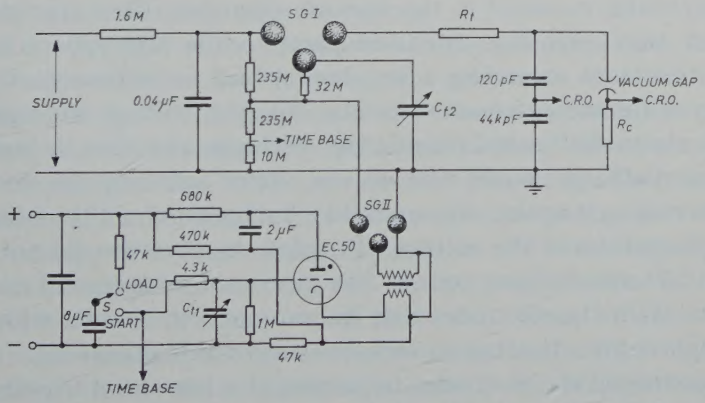

Fig. 4. Impulse generator with starting circuit (see text).

The thyratron was fired at a time interval after a starting impulse had been given to the time base of the cathode ray oscilloscope (c.r.o.) by switching S from load to start position. This time interval could be adjusted by the condensor C_{t1}. However, it had a minimum value, owing to the self-inductance of the induction coil. Therefore, for small rise times (< 10 μs), the time base was started by a pulse taken from a resistor (10 MΩ) in series with the voltage divider on the supply condensor (0.04 μF). The delay then could be adjusted by the small variable high-voltage condensor C_{t2}.

The gap voltage was measured with a capacitive voltage divider, the largest condensor of which was specially constructed to have a negligible self-inductance in order to avoid false readings at small risetimes.

Current was measured by means of a low-inductance 10 kΩ resistor. All measuring voltages were photographically recorded with a c.r.o.

§ 3. *Conditioning of the electrodes.* Before mounting, the electrodes were polished, washed in benzene and then in destilled water. Care was taken not to touch the electrode surfaces after cleaning.

Outgassing of the electrodes was done by induction heating to a temperature of well over 700°C for 5 to 6 hours. In the all-glass system the electrodes could be heated in situ, but the electrodes of the demountable vessel had to be outgassed outside the vessel. This was done in special glass containers connected to the pumping system. After heat treatment, these containers were broken and the electrodes mounted in the vacuum chamber. The experiments showed that exposing outgassed parts to the atmosphere for a short time (not exceeding a few hours) had no influence on the results of the measurements (see also [14])). If a voltage was applied to the electrodes heated outside the discharge chamber, a kind of gaseous discharge would first appear. After lowering the voltage and increasing it again, only spark-like discharges could be observed at higher values of the voltage. Provided the pressure did not rise above 0.01 mm for long periods, the gaseous discharges did not reappear. With the electrodes that did not come in contact with the atmosphere after heating no such discharges were observed.

Degassing of the electrodes by means of a low-current hydrogen discharge (5 mA) at pressures from 0.1 to 1.0 mm Hg has also been

tried (gap setting 3 mm). Preliminary a.c. experiments showed, however, that increasing the voltage across the gap always resulted in a gaseous discharge of high intensity, either in the space between the electrodes or in the whole vessel. These discharges caused the pressure in the vessel to increase considerably, sometimes to as much as a hundredfold of the initial pressure. Better results might be expected if the current in the hydrogen discharge were much larger (order of 1 A; see [7]).

For the first few voltage runs, small sparks were always observed between freshly mounted well-degassed electrodes, at relatively small values of the voltage (about 10 kV at 2 mm gap width). These sparks had the appearance of tiny red to white hot particles crossing the gap and hardly affected the gap voltage (a.c. experiments). These are probably small pieces of electrode material, weakly attached to the surface as a result of the previous machining, that are torn loose by electrostatic forces [9]). Later on, these sparks no longer appeared with the same set of electrodes, except sometimes in the voltage interval just prior to breakdown (see § 5).

§ 4. *Impulse voltage breakdown* (*all-glass system, stainless steel electrodes*).

4.1. Breakdown voltage. The effect of the following items on the breakdown strength of a 0.1 mm gap has been investigated:

a) preceding breakdowns,

b) the time interval between the breakdown under observation and the foregoing one,

c) the rise time of the impulse voltage.

4.1.*a*. A graph of the breakdown voltage V_b versus the number of breakdowns after the mounting of a particular set of electrodes is shown in fig. 5. This graph holds for a series of breakdowns with a time interval between the discharges of 30 s. This interval also has an effect on the breakdown voltage (see 4.1.*b*). Therefore the number of breakdowns, required to reach the maximum value of the breakdown voltage again, depends on the time elapsed since the last breakdown occurred and on the total number of breakdowns made on the same set of electrodes. Thus, for much used electrodes that had not been experimented with for a few days the maximum level was reached after about 10 breakdowns. For relatively new electrodes this number is much larger (fig. 5).

It may be noted that, once a few tens of discharges had been made, the low initial value of the breakdown strength of new electrodes never occurred again with the same set. Apparently the conditioning of the electrodes by discharges has a permanent and a temporary component, the temporary conditioning of much used electrodes being achieved with fewer discharges than that of less used electrodes.

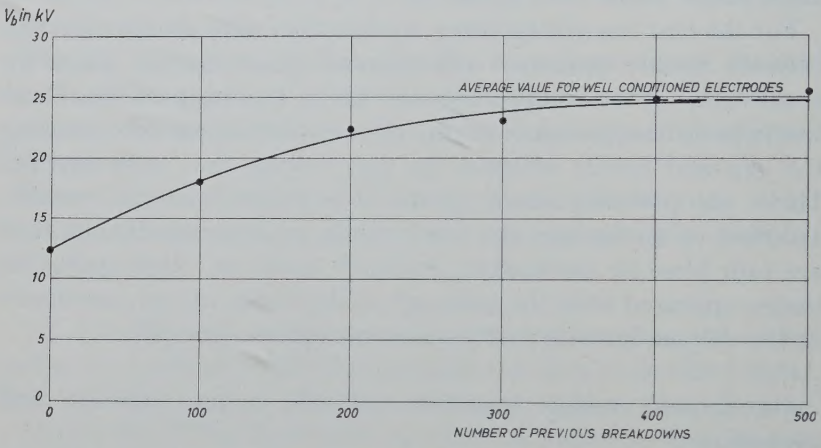

Fig. 5. Breakdown voltage V_b as a function of the number of previous discharges. Iron electrodes, $d = 0.1$ mm. Rise time to breakdown 5.10^{-4} s.

4.1.*b*. Some experiments have been performed to estimate the time in which the temporary conditioning is lost while maintaining vacuum conditions. A gap between two well-conditioned electrodes showed a decrease in the breakdown voltage if the time interval between two successive discharges was of the order of 1 minute or longer and the rise time of the voltage was less than, say, 40 μs (table I). With a larger rise time, the time interval between successive breakdowns could be increased to between 5 and 15 minutes before a decrease in the breakdown voltage was obtained (table II). Time intervals of more than 5 hours caused a further decrease to about the minimum breakdown voltage found with much used electrodes.

Table I shows a comparison between maximum breakdown voltage and breakdown voltage after 5 minutes for different values of the rise time (average of 3 observations for each rise time).

TABLE I

A (μs)	*B* (kV)	*C* (kV)	
2	23 ± 0.8	20 ± 0.9	Some influence of 5
5	19 ± 2.2	16 ± 1.0	min time interval
20	24 ± 1.7	21 ± 0.6	
40	26 ± 1.0	26 ± 0.9	No influence of 5
85	27 ± 0.8	27.5 ± 0.5	min time interval
220	27 ± 0.8	26.5 ± 0.7	

A = rise time to breakdown.
B = maximum breakdown voltage (11th discharge of a series with an interval of 15 *s* between successive discharges).
C = breakdown voltage 5 minutes after *B*.

TABLE II

	A	*B*	*C*
1	5 min	22.5 kV	26.7 ± 1.0 kV
2	15 ,,	22.5 ,,	25.2 ± 0.4 ,,
3	30 ,,	19.5 ,,	25.9 ± 0.9 ,,
4	60 ,,	24.0 ,,	26.5 ± 0.7 ,,
5	2 h	22.5 ,,	25.8 ± 1.2 ,,
6	3 ,,	20.5 ,,	26.8 ± 0.5 ,,
7	4 ,,	21.5 ,,	25.4 ± 1.1 ,,
8	5 ,,	22.0 ,,	25.0 ± 1.0 ,,
9	6 ,,	17.5 ,,	25.7 ± 1.1 ,,
10	7 ,,	17.0 ,,	25.3 ± 1.2 ,,

A = time interval after the preceding series (having maximum values of the breakdown voltage).
B = breakdown strength of the first discharge in a series.
C = mean breakdown strength of the following 5 discharges (caused within 5 minutes).

Table II, column *B*, shows the reduction that occurs in the breakdown voltage of the first breakdown after the time intervals mentioned in column *A* (rise time to breakdown 1.2 ms). From column *C* it appears that the average value of the breakdown voltage in the next five discharges is again equal to the maximum attainable value. This indicates a rapid re-conditioning of the electrodes after a temporary deterioration.

It has to be added that if the discharges are forced to follow each other with time intervals of less than about 1 ms, then the first of such a series generally shows the highest breakdown voltage. This is shown by six series of rapidly following discharges with the rise time of the voltage up to 20 kV equal to 0.48 ms. The average breakdown voltage of the first discharges of each series was 22.3 ±

0.6 kV, whilst the average breakdown strength of 32 following discharges (taken from all six series) was 18.5 $\pm$ 3.1 kV. For 6 series with the rise time of the voltage to 20 kV equal to 0.13 ms these figures were 24.3 $\pm$ 0.8 kV and 20.9 $\pm$ 1.7 kV (average of 41 discharges) respectively. Such a rapid succession can be forced by placing a suitable resistor in series with the gap.

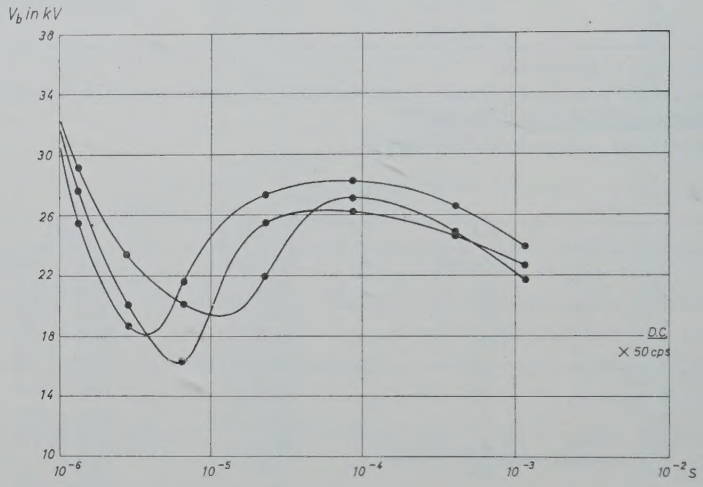

Fig. 6. Breakdown voltage V_b versus the rise time of the voltage. The breakdown voltage for 50 Hz. alternating voltage is indicated by (X). Stainless steel electrodes. d = 0.1 mm.

4.1.*c*. The relation between breakdown voltage and rise time is shown in fig. 6, where three series of observations with different rise times are plotted. To make sure that the conditioning of the electrodes would be approximately the same for the different series (taken on different days), 50 discharges were caused just before the beginning of each series. The breakdown voltages in the series were each taken from the last one of a sequence of ten breakdowns, closely following each other (invervals of 30 s).

The average value of a few observations with slowly increasing direct voltage (1 kV/s) and the maximum breakdown voltage with 50 Hz alternating voltage are indicated on the same graph. The breakdown voltage initially decreases with increasing rise time to a minimum at about 5×10^{-6} s; it then rises until a maximum occurs between 5×10^{-5} and 1×10^{-4} s; after that it slowly falls

again. For the shortest rise times and those longer than 5×10^{-5} s, the spread in the measuring series is considerably less than that around the minimum.

4.2. Pre-breakdown current. The pre-breakdown current consists of a leading capacitive component and a component in phase with the applied voltage. The latter can be found by subtracting the (calculated) capacitive component from the total current. This apparently leads to inaccuracies at the beginning of the appearance of the pre-breakdown currents, where the capacitive current has its highest value.

As table III shows, the current intensity, just before breakdown is initiated, increases with the number of breakdowns as long as the maximum level in the breakdown voltage has not yet been reached. Once the maximum breakdown voltage has been reached, this current remains of the same order; variations of 20 to 30% may occur.

TABLE III

(Rise time: 0—30 kV in 250 μs)

A	*B*	*C*
1	135 μA	19.5 kV
2	150 ,,	23.2 ,,
3	150 ,,	23.2 ,,
4	180 ,,	23.7 ,,
5	200 ,,	24.0 ,,
10	600 ,,	26.8 ,,
19	240 ,,	25.0 ,,
20	450 ,,	25.9 ,,
21	600 ,,	26.8 ,,
36	1200 ,,	27.2 ,,
37	1050 ,,	27.0 ,,
38	1100 ,,	27.2 ,,

A = number of discharges
B = current just prior to breakdown
C = breakdown voltage

For higher numbers of discharges the current remains in the order of 1 mA. The current-voltage relation prior to breakdown for different rise times is given in fig. 7. Because of the large capacitive component of the observed current, the values of the curves for the two smallest rise times are not very reliable, except for those parts

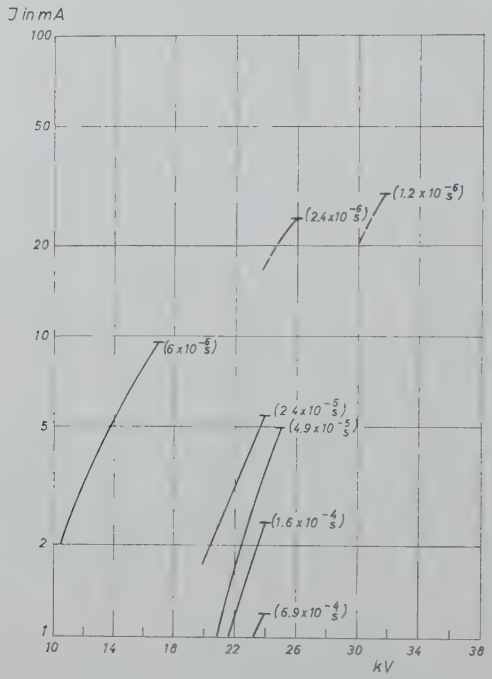

Fig. 7. Current-voltage relations for different rise times of the impulse voltage (indicated in brackets). Stainless steel electrodes, $d = 0.1$ mm.

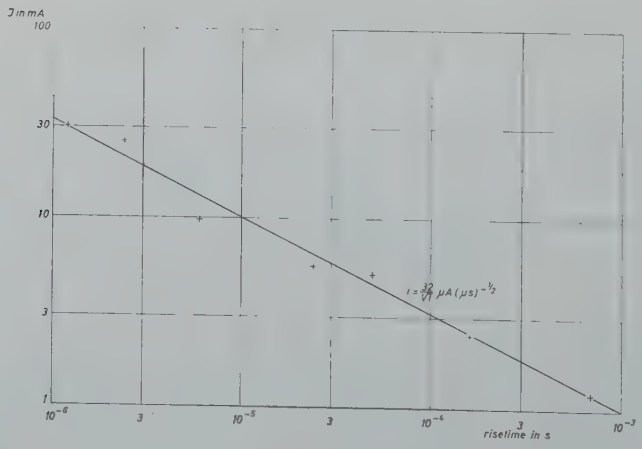

Fig. 8. Current just before breakdown as a function of the rise time of the voltage. Stainless steel electrodes, $d = 0.1$ mm.

just prior to breakdown. For a rise time of 1 μs the current increases to 30 mA before breakdown occurs. With increasing rise time, the current intensity just before breakdown decreases inversely proportional to $\sqrt{t}$ (fig. 8). The energy flux into the electrodes, calculated from the observations given in fig. 8, is in first approximation proportional to $\sqrt{t}$ (assuming that the fraction of the total energy which penetrates into the electrodes is independent of the voltage). The heat flow from a source of high temperature, situated on the electrode surface, into its volume is also proportional to $\sqrt{t}$ (ref. [18]), p. 91). Hence, it seems that a critical energy flux to the anode is needed to initiate the discharge.

Current observations showed that sometimes the current would increase when in the tail of the voltage wave the voltage was already decreasing. While in some cases breakdown followed, this was not always the case. The final transition from pre-breakdown current to discharge current (not visible on most photographs) happened in a very short time that is estimated to be less than 10^{-7} s.

The appearance of the electrode surfaces after many breakdowns showed that a large amount of anode material was deposited on the cathode (fig. 9). Only a negligible amount of material left the gap by radial diffusion. A minor part of the anode material appeared as droplets on the cathode surface which were rather weakly attached and easily removed. From the colours of the electrodes it appeared that the whole of the anode had reached far higher temperatures than the cathode.

4.3. Conclusions. The experiments described in §§ 4.1 and 4.2 have shown that the electrode surfaces are best conditioned by a series of breakdowns. Apparently these surfaces are changed by the evaporation of projections. This lowers the effective field strength at the electrode surface and decreases the effective absorbing surface, thereby affecting any surface layers. This leads to permanent conditioning. Temporary conditioning is caused by removing the surface layers.

These are re-formed after a time which can be deduced from table II. Obviously the removal of the surface layers also takes place before breakdown. This makes it understandable that for the shorter rise times less time is needed to lower the breakdown

voltage than for the larger rise times. The energy needed to remove the surface layers, delivered before breakdown takes place, will be small at short rise times, thus only allowing the removal of an incomplete (formed in a short time) surface layer.

Analogous reasons can explain the dependence of the breakdown voltage on the rise time of the voltage. For very short rise times the breakdown voltage can be expected to be high because, again, only a small amount of energy is produced at the electrode surface. For a

Fig. 9. Appearance of the electrodes after a large number of discharges (impulse voltage). Left: anode.

rise time of 1 μs the pre-breakdown current must grow to about 30 mA in order that sufficient anode material is evaporated for discharge initiation. Thus, for increasing rise times one would expect the breakdown voltage to fall. It is thought however, that a second process runs parallel with the first mentioned, this second process being the pre-breakdown removal of surface layers that tend to decrease the breakdown voltage. The pre-breakdown removal of surface layers is thought to commence in the region of 5 μs. This initially results in an increase of the breakdown voltage with longer

rise times. If the rise time is larger than about 100 μs, the cleansing effect is no longer affected by the rise time and the breakdown voltage gradually decreases to its final (d.c.) value.

§ 5. *Measurements with* 50 Hz *alternating voltage.*

5.1. Breakdown voltage. The breakdown voltage as a function of gap width for well-conditioned iron and copper electrodes is given in fig. 1, curve 7*a* and 7*b* resp. The breakdown voltage is defined here as the voltage at which a spark between the electrodes is observed if the voltage is slowly increased from zero to its final value.

The spread in the observed breakdown voltages is influenced by the number of preceding breakdowns and by the time in which the voltage is adjusted from zero to the value at which breakdown occurs.

Although the applied induction heating was sufficient to avoid discharges in gas liberated from the electrode surfaces, the main conditioning in order to obtain maximum breakdown voltages was done by previous discharges (see also § 4). These maximum values showed an average spread of about 8% for several measuring sequences. Even with well-conditioned electrodes, however, deviations to values as low as 40% of the maximum breakdown strength occasionally occurred.

Electrodes not fully conditioned by previous discharges in general showed a lower breakdown voltage with faster increase of the applied voltage. Here also the pre-breakdown currents appear to have a conditioning influence.

5.2. Pre-breakdown current. Contrary to the experiments described in § 4.2, the voltage in the a.c. experiments could be maintained during a longer time at an arbitrary value below the breakdown voltage. This facilitated the measurement of current and voltage, but on the other hand introduced phenomena which influenced the pure vacuum breakdown, e.g., strong heating of the electrodes.

Around the voltage where field emission becomes noticeable by the occurrence of peaks on the current records (fig. 10*a*), small red to white glowing spots appeared on the electrode surfaces. On raising the voltage, the number of these spots increased, whilst a

pale blue disk with a diameter of a few mm developed at the middle of each electrode surface. In the voltage interval just prior to breakdown these disks grew out to a transparent luminous channel connecting the electrodes. In this channel occasionally red glowing particles could be observed, crossing the gap.

In most cases field emission from one electrode started at a lower voltage than from the other (fig. 10*a*), whilst initially the luminous phenomena also appeared on one electrode only. From the sign of the peaks on the current records it could be concluded that this occurred on the electrode emitting least. Apparently the glowing spots were caused by a bombardment of field-emission electrons. Some d.c. experiments confirmed this assumption. It should be noted that a strong X-ray radiation was measured during these experiments.

At a much higher current (about 4 mA) some extreme cases have been observed, at which the whole of one of the electrodes was heated to a bright red glow without breakdown occurring. Exchange of electrodes proved this to be due to the "cold" electrode, which on the oscillograms also showed the largest field-emission currents.

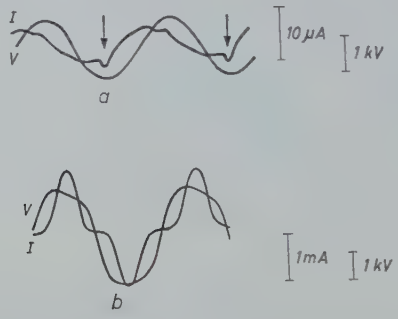

Fig. 10. Pre-breakdown current and gap voltage for 50 Hz voltage. Copper electrodes, $d = 0.1$ mm.

a) Peaks on the curve of current vs time caused by field emission (arrows).
b) Current rising independently of the voltage.

With a large series resistor (1.56 MΩ) it was found that from certain values upwards the current could rise with decreasing voltages as shown in fig. 10*b*. It may be noticed that the current intensity through the gap measured in this case is larger than was found in the impulse voltage experiments just before breakdown (fig. 8).

This can be explained by assuming that some gas multiplication occurs in the vapour of an electrode hotspot, which, however, is not enough to lead to breakdown, firstly because the voltage is too low and secondly because there is no reason to suppose that in this case the current density will be high. This assumption is confirmed by the fact that the current may grow with decreasing voltage. With alternating current, hotspots on any of the electrodes can be formed during the voltage rise with less energy than with impulse voltage because the electrodes can be pre-heated by the preceding voltage cycles.

This section so far has only dealt with experiments in the demountable vacuum chamber. In the all-glass system some comparative experiments concerning pre-breakdown currents have been carried out. The same phenomena occurred here, except for some quantitative differences:

a) At a given voltage the spread in the current values is larger in the all-glass system,

b) At a given voltage the mean value of the current is larger in the all-glass system.

It proved that the spread in the current-voltage curves is mainly due to taking data from experiments with different peak voltage values. A greater peak value giving a current-voltage curve that has shifted to lower values of the current. This is probably due to the more effective conditioning of the electrodes with high voltages and currents in the preceding voltage loops. Nevertheless, even if this effect is taken into account, the differences mentioned under *a*) and *b*) still exist. The principal difference between the two set-ups might be the diffusion pump used. It is thought that oil-vapours resulting from the oil diffusion pump contaminate the electrode surfaces in such a way as to lower the average effective work function.

Finally the influence of the time interval after the induction heating of the electrodes has been investigated. Current data were compared from:

a) cold electrodes, heated more than 24 hours ago.
b) cold electrodes, heated less than half an hour ago.
c) electrodes with a temperature of about 700°C.

All data were taken with the same peak value of the alternating voltage. In the order of the different heat treatments mentioned above, the current intensity slightly diminished (at the same value

of the voltage). However, the differences obtained were smaller than the spread caused by taking values of the current at different peak values of the alternating voltage.

§ 6. *Discussion.* Some conclusions deduced from the results dealt with in §§ 4 and 5 have been given in § 4.3 and § 5.2 respectively. Although our investigations cannot provide all information needed for the complete understanding of the mechanism of vacuum breakdown in our experimental circumstances, it seems most probable that heating of the anode by field-emission electrons followed by evaporation of parts of the anode surface is the main factor initiating breakdown (§ 1, assumption *a*).

It was observed that a luminous phenomenon and a high temperature at the anode is reached at a lower voltage than at the cathode. This is confirmed by observations with an ultra high-speed camera by Chiles [19]), who also recorded the speed of the vapour stream leaving the anode (5×10^5 cm/s, impulse voltage experiments).

It is less probable that heating of the cathode to a temperature where evaporation occurs should play a part in the initiation of breakdown (§ 1, assumption *b* and *c*). In that case one would expect that the projections which provide the field-emission electrons should always come into the same emission conditions, because these points are heated most. Consequently the different current-voltage relationships, given in fig. 7 should all coincide. However, it is repeatedly proved by our experiments that the effective work-function of the cathode tends to lower values for shorter rise times (shift of the curves in fig. 7 to the left). A possible explanation has been given in § 4.3 (removal of surface layers).

From the observed luminous phenomena in a.c. experiments (§ 5.2) and from fig. 10*b* it appears that excitation and ionisation of vapour liberated at the anode already exists before the actual (sudden) breakdown takes place. The latter, then, might occur only when the vapour density passes a critical value. Fig. 10*b* might be explained by assuming that as the temperature of the electrodes is still increasing during the fall of the voltage, the vapour density also increases, thereby giving the current a chance to grow to a value limited by the series resistor. At higher voltages the vapour density might reach a value sufficiently high to start a multipli-

cation process resulting in a sudden increase of the current (breakdown).

The hypothesis that a critical energy flux to the anode is needed to initiate a discharge (§ 2.4) seems to be contradicted by the fact that, for electrodes not completely conditioned, breakdown occurs at low voltage and also at low pre-breakdown current (§ 4.2, table III). From a comparison of the current-voltage relationship in the a.c. experiments with the Fowler-Nordheim equation for the field-emission current density it appears, however, that clean cathode surfaces with a high effective work-function have a larger emitting surface than those with lower effective work-function. This means that on the less conditioned electrode surfaces there are only a few points that contribute to the emission of field electrons, thus giving a high current density, whilst the total current may be relatively low.

As for Cranberg's theory (§ 1, item *d*), it seems unlikely that the observed irregular appearance of pieces of material alone is sufficient to cause breakdown at the well reproduceable voltage values found here. On the other hand it is possible that this theory holds for the casual occurrence of breakdown in large gaps, where at high voltages discharges can be initiated with irregular intervals of up to several hours.

Acknowledgements. The author wishes to thank Prof. Dr. D. Th. J. ter Horst, now at the Technische Hogeschool Eindhoven, and Dr. G. A. W. Rutgers of the Research Department of N.V. K.E.M.A. for their interest, valuable advice and stimulating discussions during the course of this work.

Received 21th July, 1960.

REFERENCES

1) Myers, O. F. and W. A. Raatz, U.S.A.E.C.; LRL — 158, 1955.
2) Boyle, W. S., P. Kisliuk, and L. H. Germer, J. Appl. Phys. **26** (1955) 720.
3) Ahearn, A. J., Phys. Rev. **50** (1936) 538.
4) Dyke, W. P. and J. K. Trolan, Phys. Rev. **82** (1951) 575; Phys. Rev. **89** (1953) 799.
5) Dyke, W. P., J. K. Trolan, E. E. Martin, and J. P. Barbour, Phys. Rev. **91** (1953) 1043.
6) Dolan, W. W., W. P. Dyke, and J. K. Trolan, Phys. Rev. **91** (1953) 1054.

7) Denholm, A. S., Can. J. Phys. **36** (1958) 476.
8) Chambers, C. C., J. Franklin Inst. **218** (1934) 463.
9) Cranberg, L., J. Appl. Phys. **23** (1952) 518.
10) Van Atta, L. C., R. J. van de Graaff and H. A. Barton, Phys. Rev. **43** (1933) 158.
11) McKibben, J. L. and R. K. Beauchamp, U. S.A.E.C., AECD—2039, 1948.
12) Trump, J. G. and R. J. van de Graaff, J. Appl. Phys. **18** (1947) 327.
13) Webster, E. W., R. J. van de Graaff and J. G. Trump, J. Appl. Phys. **23** (1952) 264.
14) Dushman, S., The scientific Foundations of Vacuumtechnique, John Wiley and Sons Inc., New York 1949, pp 631–635.
15) Mason, R. C., Phys. Rev. **52** (1937) 126.
16) Leader, D., Proc. Instn Elect. Engrs **100** (IIa) (1953) 138.
17) Rosanova, N. B. and V. L. Granovskii, Sovjet Physics, Techn. Phys. **1** (1956) 471.
18) Ingersoll, L. R., O. J. Zobel and A. C. Ingersoll, Heat conduction, The University of Wisconsin Press 1954, Ch. 7.
19) Chiles, J. A., J. Appl. Phys. **8** (1937) 622.

Appl. sci. Res. Section B, Vol. 9

A CLASS OF BOUNDARY VALUE PROBLEMS

by W. E. WILLIAMS

Department of Applied Mathematics, Liverpool University, England

Summary

A simple method is presented for the solution of the partial differential equation of diffusion type with constant values of the solution or its normal derivative prescribed on the surfaces of a wedge of arbitrary angle. It is shown that this solution may be transformed in such a manner that it yields the solution to a similar class of boundary value problems for the time-harmonic wave (i.e. Helmholtz's) equation. Direct solutions are also obtained for the problem of the diffraction of acoustic or electromagnetic plane waves by a perfectly absorbing or a perfectly reflecting wedge. In one solution the difraction problem is solved by modifying the solution of a similar boundary value problem for the diffusion equation. In the second formulation the solution of the diffraction problem is obtained by expressing the total solution as a sum of a diffracted field and geometrical optics terms. The diffracted field is then obtained by imposing the conditions of continuity across the shadow lines of geometrical optics. The solution for the diffraction of an arbitrary plane pulse by a wedge is also obtained; the solution being valid even if the boundary conditions are of the impedance type.

§ 1. *Introduction.* For over fifty years the solution of the diffusion and time harmonic wave (i.e. Helmholtz's) equations with conditions specified on wedge surfaces has attracted the interest of a large number of investigators. Boundary value problems of this nature occur in a number of different physical situations, and many different methods of solution have been considered. The object of the present work is to present a simple unified approach to the solution of a class of problems of this type. Before considering the techniques and problems examined in the present paper we shall review briefly the main methods used in the solution of boundary value problems on wedge and the physical situations which produce such problems.

The problems for Helmholtz's equation are mainly in acoustic and electromagnetic diffraction, the main interest having been concentrated on diffraction of plane waves by perfectly reflecting or perfectly absorbing wedges. The earliest solution is that of Sommerfeld [1]) who employed the method of images on a Riemann sheet for a wedge of angle 2π. This approach was employed by Carslaw [2]) who also obtained the Green's functions for arbitrary wedges. An alternative approach to this type of diffraction problem is that of Macdonald [3]) who obtained the solution as an infinite series of Bessel functions. Another different method is that of Kontorovich and Lebedev [4]) who employed integral transforms of Hankel and Bessel functions with respect to their order. This approach has also been utilised by Oberhettinger [5]) in deriving the Green's functions for wedges. Diffraction problems for wedges with impedance conditions prescribed on the surfaces have been considered by the author [6])[7]), the solution being effected by employing a suitable contour integral representation. This type of problem has also been solved by Senior [8]) and by Maliuzhinets [9]) (the author has not seen this thesis).

Another class of problems for Helmholtz's equation which has attracted some interest is that when the solution or its derivative is prescribed on the wedge surfaces. The simplest case is when the prescribed values on the surface are constant; clearly one method of obtaining a solution is by employing the Green's function. This latter function is rather complicated, and it seems desirable to use a more direct approach. Such an approach has been developed by Maliuzhinets [10]) who considers acoustic radiation from a wedge whose surfaces are oscillating with a constant velocity. His approach consists of using a contour integral representation and reducing the problem to solving an inhomogeneous difference equation. This latter equation is similar to one occurring in the problem of diffraction by a metallic wedge [6]), and the solution is rather complicated. By employing certain properties of this solution Maliuzhinets shows that the solution for the radiation problem may be expressed as a real integral involving trigonometrical and hyperbolic functions. The solution of the difference equation does not occur explicitly, and it thus seems that the introduction of this function is superfluous and that a more direct approach is feasible.

The main boundary value problem for the diffusion equation

with constant values prescribed on wedge surfaces is the Rayleigh problem for a wedge in an incompressible fluid. Basically this problem is time dependent, but a Laplace transform reduces the basic equation to that of diffusion. A solution of this problem has been given by Hasimoto [11]; his method involves a change of variable and a solution then obtained, by separation of variables, in terms of an infinite series of confluent hypergeometric functions. A suitable contour integral representation of these functions reduces the solution to a more suitable form. For wedge angles an integral sub-multiple of π a solution has been given by Sowerby [12], who employed the known Green's function [2] for the problem. This approach was subsequently generalized to a wedge of arbitrary angle by Sowerby and Cooke [13]. The same type of boundary value problem occurs in the theory of heat conduction, and in this case a solution has been given by Jaeger [14] as an infinite series of Bessel functions. A similar boundary value problem occurs in the theory of neutron absorption, and a solution was obtained by Levine [15] by means of the Kontorovich-Lebedev transform. A solution to this problem employing the Green's function has been given by Lauwerier [16].

In most of the above examples the final solution is relatively simple, though the intermediate calculations may be lengthy and involve complicated functions. It is thus clearly desirable to obtain a simple method of formulation which enables the above and more complicated problems to be solved in a simple and direct manner.

In § 2 we consider the solution of the diffusion equation with arbitrary constant values specified on a wedge. The solution is effected by employing a real integral representation for the solution which was first used by Van Dantzig [17]. A simple application of the theory of distributions [18] or of generalised functions [19] reduces the boundary value problem to the solution of a difference equation. This latter equation is solved by means of Fourier transforms, the final solution being expressed in terms of trigonometrical functions. The corresponding solution with constant values of the normal derivative prescribed on the wedge surface is also given. The approach may be applied to the case when a linear combination of the solution and its normal derivative has prescribed constant values on the two wedge surfaces. It may also be used to solve problems where such a linear combination vanishes

on one wedge surface and the function is constant on the other surface. Problems of this type occur in oceanography [20]). It is also shown that the solution obtained may, by slight manipulation, be written in such a manner that it may also be applied to obtain solutions of Helmholtz's equation. Thus solutions are immediately obtained to the type of problem considered by Maliuzhinets, and the solution obtained by the present approach agrees with that of Maliuzhinets.

In § 3 the particular type of boundary value problem occurring in acoustic and electromagnetic diffraction theory is considered. Two different methods of solution are examined. The first method is an indirect one; the approach of § 2 is used to obtain the solution of a particular type of boundary value problem for the diffusion equation. It is then shown that, by suitable re-arrangement and slight modification, the solution for the diffraction problem may be obtained. In the second approach the solution to the diffraction problem is formulated as a sum of the plane wave terms of geometrical optics and a diffracted term. A real integral representation of this term is employed, and the conditions of continuity across the shadow lines of geometrical optics yield a set of simultaneous functional equations. The solution of these is obtained as in § 2. The approach may also be used to solve problems where impedance conditions are prescribed on the wedge surfaces. The only difference in these problems is that the functional equation to be solved is more complicated.

The particular form of the solution obtained by this second approach is particularly suitable for the solution of diffraction by plane pulses of arbitrary shape. The solution for the time-dependent problem may be written down immediately from the time-harmonic solution if the boundary conditions on the wedge surface are of the form (time derivative on surface/normal derivative on surface) = constant. This type of problem has been considered by Papadopoulos [21]), for the particular case of a half-plane, by assuming dynamic similarity. It is also of interest to note that the diffraction problem for the time-dependent wave equation may be formulated directly without recourse to the time-harmonic solution. The solution is once more expressed as the sum of geometrical optics terms and a diffracted term. The only difference lies in the integral representation of the diffracted term; the formal steps in the

analysis and the difference equations are exactly as for the time harmonic case. This approach seems to present a more direct and simpler approach to these problems than that of Keller [22]) or Papadopoulos [23]). It also has the advantage that it is not restricted to unit step function pulses.

§ 2. *Simple solutions of the diffusion equation.* Throughout the present work we shall be concerned with the region of physical space outside a wedge of angle α. If (r, ϑ) denote cylindrical polar coordinates with axis parallel to the edge of the wedge, the region of space of interest is defined by $0 \leq r \leq \infty$, $0 \leq \vartheta \leq \alpha$. In the present section we shall obtain the solution of two simple boundary value problems for the equation

$$(\nabla^2 - k^2)\phi = 0, \tag{1}$$

where

$$\nabla^2 = \frac{\partial^2}{\partial r^2} + \frac{1}{r}\frac{\partial}{\partial r} + \frac{1}{r^2}\frac{\partial^2}{\partial \vartheta^2}$$

and k is real. The first problem is the determination of a solution $\phi_1(r, \vartheta)$ of (1) such that $\phi_1 = 1$ on $\vartheta = 0$, $\phi_1 = 0$ on $\vartheta = \alpha$ and $\phi_1 \to 0$ as $r \to \infty$ in $0 < \vartheta \leq \alpha$. The second problem is that of obtaining a solution $\phi_2(r, \vartheta)$ with $r^{-1}\partial\phi_2/\partial\vartheta = 1$ on $\vartheta = 0$ and $r^{-1}\partial\phi_2/\partial\vartheta = 0$ on $\vartheta = \alpha$; ϕ_2 satisfies the same conditions as ϕ_1 at infinity. Clearly from ϕ_1, ϕ_2 we can construct a solution of (1) with values c_1, c_2 on $\vartheta = 0$ and α respectively, such a solution is $c_1\phi_1(r, \vartheta) + c_2\phi_1(r, \alpha - \vartheta)$. From these functions ϕ_1, ϕ_2 solutions can be obtained for the Rayleigh problem for an incompressible fluid [11]) and for problems in heat conduction treated by Jaeger [14]). In both these problems k will involve a Laplace transform parameter. The solution to the diffusion problem treated by Levine [15]) may also be obtained. We shall not consider the application of our results to these particular problems but merely obtain the solutions.

These solutions will be obtained by employing an integral representation for solutions of (1). The most convenient for the present problem is that of Van Dantzig [17]). We thus have

$$\phi_1 = \int_{-\infty}^{\infty} e^{-ikr\sinh\eta}\{F_1[\eta + i(\vartheta - \alpha)] - F_1[\eta - i(\vartheta - \alpha)]\}d\eta. \tag{2}$$

$F_1(\eta)$ is an arbitrary function, analytic in the strip $-\alpha < \operatorname{Im}\eta < \alpha$,

and the form of ϕ_1 is such that the conditions on $\vartheta = \alpha$ are automatically satisfied. The condition on $\vartheta = 0$ gives

$$\int_{-\infty}^{\infty} e^{-ikr\sinh\eta} [F_1(\eta - i\alpha) - F_1(\eta + i\alpha)]d\eta = 1. \quad (3)$$

The part of the integrand in square brackets in (3) clearly does not represent a function in the normal sense, but nevertheless it may be interpreted as a generalised function [19]) or as defining a distribution [18]). In either case its Fourier transform may be defined. For convenience the symbolic notation of the delta function will be employed and thus

$$F_1(\eta - i\alpha) - F_1(\eta + i\alpha) = \delta(\eta). \quad (4)$$

Equation (4) may be solved by conventional Fourier transform techniques. If $\bar{F}_1(\zeta)$ is defined by

$$F_1(\eta) = \frac{1}{2\pi}\int_{-\infty}^{\infty} \bar{F}_1(\zeta)\, e^{i\eta\zeta}\, d\zeta,$$

then (4) becomes

$$2\bar{F}_1(\zeta)\sinh\alpha\zeta = 1.$$

Thus

$$F_1(\eta) = \frac{1}{2\pi}\int_{-\infty}^{\infty} e^{i\eta\zeta}\,\bar{F}_1(\zeta)d\zeta = \frac{i}{4\pi}\int_{-\infty}^{\infty} \frac{\sin\eta\zeta}{\sinh\alpha\zeta}\,d\zeta = \tfrac{1}{4}i\tanh\tfrac{1}{2}\alpha\tau,$$

where $\tau = \pi/\alpha$. Hence

$$\phi_1 = \frac{i}{4\alpha}\int_{-\infty}^{\infty} e^{-ikr\sinh\eta} [\coth\tfrac{1}{2}\tau(\eta + i\vartheta) - \coth\tfrac{1}{2}\tau(\eta - i\vartheta)]d\eta. \quad (5)$$

Similarly

$$\phi_2 = \frac{i}{4k\alpha}\int_{-\infty}^{\infty} e^{-ikr\sinh\eta} [\coth\tfrac{1}{2}\tau(\eta + i\vartheta) + \coth\tfrac{1}{2}\tau(\eta - i\vartheta)]d\eta. \quad (6)$$

We now apply these results to one of the boundary value problems mentioned above, namely that treated by Levine. In this case the

function ϕ is required to be unity on both surfaces and hence

$$\phi = \frac{i}{4\alpha}\int_{-\infty}^{\infty} e^{-ikr\sinh\eta}\,[\coth\tfrac{1}{2}\tau(\eta + i\vartheta) - \coth\tfrac{1}{2}\tau(\eta - i\vartheta) +$$
$$+ \coth\tfrac{1}{2}\tau(\eta + i\alpha - i\vartheta) - \coth\tfrac{1}{2}\tau(\eta - i\alpha + i\vartheta)]\,d\eta =$$
$$= \frac{i}{2\alpha}\int_{-\infty}^{\infty} e^{-ikr\sinh\eta}[\operatorname{cosech}\tau(\eta + i\vartheta) - \operatorname{cosech}\tau(\eta - i\vartheta)]\,d\eta. \quad (7)$$

Eq. (7) is identical with the result obtained by Levine; also with a suitable interpretation of the parameter k it represents the solution for the Rayleigh problem for an incompressible fluid and a wedge of exterior angle α. It should be noted that (7) could have been derived more directly by employing the properties of symmetry which require that $\partial\phi/\partial\theta = 0$ on $\vartheta = \frac{1}{2}\alpha$.

It is clearly of interest to consider whether the above results may be employed to obtain solutions of

$$(\nabla^2 + k^2)\phi = 0 \quad (8)$$

with either ϕ or its derivative having prescribed constant values on the wedge surface. Boundary value problems of this nature occur in acoustics and electromagnetic theory in determining solutions of the time-harmonic wave equation with prescribed conditions on a boundary. Formally at least one would expect to obtain a solution of (8) from that of (1) by replacing k by ik. Clearly equations (5) and (6) are such that the integrals diverge for k purely imaginary, and thus it is necessary to re-write these in a form which is valid for such values of k.

We have that

$$\phi_1 = \frac{i}{4\alpha}\int_{-\infty+\frac{1}{2}\pi i}^{\infty+\frac{1}{2}\pi i} e^{-kr\cosh\eta}[\coth\tfrac{1}{2}\tau(\eta - i\tfrac{1}{2}\pi + i\vartheta) - \coth\tfrac{1}{2}\tau(\eta - \tfrac{1}{2}i\pi - i\vartheta)]\,d\eta =$$
$$= \frac{i}{8\alpha}\left\{\int_{-\infty+\frac{1}{2}\pi i}^{\infty+\frac{1}{2}\pi i} e^{-kr\cosh\eta}[\coth\tfrac{1}{2}\tau(\eta - i\tfrac{1}{2}\pi + i\vartheta) - \coth\tfrac{1}{2}\tau(\eta - \tfrac{1}{2}i\pi - i\vartheta)]\,d\eta - \right.$$
$$\left. - \int_{-\infty-\frac{1}{2}\pi i}^{\infty-\frac{1}{2}\pi i} e^{-kr\cosh\eta}[\coth\tfrac{1}{2}\tau(\eta + i\tfrac{1}{2}\pi - i\vartheta) - \coth\tfrac{1}{2}\tau(\eta + \tfrac{1}{2}i\pi + i\vartheta)]\,d\eta\right\}. \quad (9)$$

Both contours of integration in (9) may be deformed to the real axis; some poles of the integrand may be captured in this deformation. Thus (9) becomes

$$\phi_1 = \sum_{n=0}^{\left[\frac{1}{2\alpha}(\frac{1}{2}\pi-\vartheta)\right]^-} \exp[-kr\sin(\vartheta+2n\alpha)] - \sum_{n=\left[\frac{\vartheta}{\alpha}\right]^+}^{\left[\frac{1}{2\alpha}(\frac{1}{2}\pi+\vartheta)\right]^-} \exp[-kr\sin(\vartheta-2n\alpha)] + \\ + \frac{i}{2\alpha}\int_0^\infty e^{-kr\sinh\eta}\,\frac{\sinh\tau(\eta+i\vartheta)}{\cosh\tau(\eta+i\vartheta)-\cos\frac{1}{2}\pi\tau}\,d\eta. \quad (10)$$

The notation $[x]^\pm$ refers to the nearest integer less than, or greater than, x respectively.

Similarly it can be shown that

$$\phi_2 = \frac{1}{k}\left\{\sum_{n=0}^{\left[\frac{1}{2\alpha}(\frac{1}{2}\pi-\vartheta)\right]^-} \exp[-kr\sin(\vartheta+2n\alpha)] + \right. \\ \left. + \sum_{n=\left[\frac{\vartheta}{\alpha}\right]^+}^{\left[\frac{1}{2\alpha}(\frac{1}{2}\pi+\vartheta)\right]^-} \exp[-kr\sin(\vartheta-2n\alpha)]\right\} - \\ - \frac{1}{2\alpha k}\sin\tfrac{1}{2}\pi\tau\int_0^\infty \frac{e^{-kr\cosh\eta}}{\cosh\tau(\eta+i\vartheta)-\cos\frac{1}{2}\pi\tau}\,d\eta. \quad (11)$$

k may now be replaced by ik in (10) and (11), and the functions so obtained will represent solutions of (8) satisfying the same boundary conditions as ϕ_1 and ϕ_2 on the wedge surface. The resulting functions will, apart from the plane wave terms, satisfy the radiation condition

$$\lim_{r\to\infty} r^{\frac{1}{2}}(\partial\phi/\partial r + ik\phi)$$

and thus, in terms of solutions of the time-harmonic wave equation, will represent outgoing waves with time dependence $\exp ikct$ where c is the wave velocity. The solution appropriate to the time dependence $\exp(-ikct)$ is obtained by replacing k in (10) and (11) by $-ik$.

Maliuzhinets [10] has considered the solution ϕ of (8) with $r^{-1}\partial\phi/\partial\vartheta = 1$ on $\vartheta = 0$ and $\partial\phi/\partial\vartheta = 0$ on $\vartheta = \alpha$ and, when notational changes are taken into account, the function obtained by replacing k by ik in (11) agrees with Maliuzhinets' solution.

The method used is directly applicable to problems where impedance conditions are prescribed on the wedge surface, the only difference being in the form of the difference equation (4). For example if we have $\phi_1 = 1$ on $\vartheta = 0$ and an impedance condition prescribed on $\vartheta = \alpha$, (4) becomes

$$F_1(\eta - i\alpha) - G(\eta)F_1(\eta + i\alpha) = \delta(\eta). \tag{12}$$

$G(\eta)$ is a known function of η and the impedance. The solution of (12) is

$$F_1(\eta) = \frac{iH(\eta)}{4H(-i\alpha)} \tanh \tfrac{1}{2}\tau\eta,$$

where $H(\eta)$ is an appropriate solution of (12) with the righthand side set equal to zero. Solutions of this equation appropriate to impedance conditions occurring in acoustics and electromagnetic theory have been considered by the author [6)7)]; a similar equation has been encountered by Peters [24)] and Van Dantzig [17)].

In the following section we shall consider whether the techniques of the present section are applicable to diffraction problems.

§ 3. *Diffraction by a wedge.* The basic problem in diffraction theory is the determination of a solution of (8) satisfying certain conditions on the wedge surfaces and at infinity. The condition at infinity depends on the incident field; in the present case we shall consider the incident field to be that of a plane wave. The condition at infinity is that the total solution, apart from the terms predicted from geometrical optics, satisfies a radiation condition. We shall employ the radiation condition appropriate to a harmonic time dependence $\exp ikct$. The conditions at the wedge depend on the physical problem considered. For example if ϕ represents the acoustic velocity potential, then $\partial\phi/\partial\vartheta = 0$ represents the condition on a perfectly hard surface and $\phi = 0$ the condition for a perfectly soft surface. If an impedance condition is to be prescribed, then $r\phi/(\partial\phi/\partial\vartheta)$ is constant on the wedge surface. Since the object of the present work is to indicate a simpler and more direct solution of these problems, it is sufficient to consider only $\phi = 0$ on the wedge surface. The solution for electromagnetic diffraction with impedance boundary conditions on the wedge surface has been obtained by a slightly different approach by the author [6)7)].

The incident wave is taken to be $\exp ikr\cos(\vartheta - \vartheta_0)$ and the total solution ϕ written as $\exp ikr\cos(\vartheta - \vartheta_0) + \chi$. One of the difficulties of diffraction theory is that it is not possible to obtain a real integral representation for χ. It is, however, possible to formulate the diffraction problem rigorously by writing ϕ as the sum of geometrical optics terms and a diffracted term which may be represented by a real integral and which is discontinuous across the shadow lines of geometrical optics. It has in fact been pointed out by Peters and Stoker [25]) that diffraction problems should be formulated in this way in order to obtain unique solutions. We shall eventually consider the solution of the diffraction problem from this rigorous viewpoint.

An alternative approach which we shall now consider is determining the solution of the diffraction problem from an appropriately formulated boundary value problem for (1). The advantage of employing (1) is that it is often possible to obtain a real integral representation of the form of (2). We therefore consider a solution χ_1 of (1) with $\chi_1 = -\exp(-ikr\sinh\lambda_1)$ on $\vartheta = 0$, $\chi_1 = -\exp(-ikr\sinh\lambda_2)$ on $\vartheta = \alpha$, λ_1, λ_2 real. The approach of § 2 gives

$$\chi_1 = \frac{1}{4\alpha i}\int_{-\infty}^{\infty} e^{-ikr\sinh\eta}[\coth\tfrac{1}{2}\tau(\eta + i\vartheta - \lambda_1) - \tanh\tfrac{1}{2}\tau(\eta + i\vartheta - \lambda_2) - \\ - \coth\tfrac{1}{2}\tau(\eta - i\vartheta - \lambda_1) + \tanh\tfrac{1}{2}\tau(\eta - i\vartheta - \lambda_2)]d\eta. \quad (13)$$

Clearly from a formal viewpoint one would expect to determine the appropriate solution χ of (8) from (13) by replacing k by ik and λ_1, λ_2 by $i(\frac{1}{2}\pi - \vartheta_0)$, $i(\frac{1}{2}\pi + \vartheta_0 - \alpha)$ respectively. We consider first the form of (13) for λ_1, λ_2 having these values; for simplicity the following discussion will be restricted to the case of $\alpha > \pi + \vartheta_0$. Any other value of α may be similarly treated.

For the above imaginary values of λ_1 and λ_2 it is clear that χ_1 vanishes on $\vartheta = 0$ and α and also the integrand is singular when $\vartheta = \frac{1}{2}\pi \pm \vartheta_0$, and we therefore consider the behaviour of χ_1 near these critical values of ϑ. Clearly this reduces to considering

$$I(\delta) = \int_{-\infty}^{\infty} e^{-ikr\sinh\eta}\coth\tfrac{1}{2}\tau(\eta + i\delta)d\eta$$

for small δ. If the infinite series for $\coth z$ is substituted into the

expression for $I(\delta)$, then we obtain

$$I(\delta + 0) - I(\delta - 0) = -4\alpha i.$$

Thus, as ϑ increases from 0 to α, χ_1 decreases by 1 across the line $\vartheta = \frac{1}{2}\pi - \vartheta_0$ and increases by 1 across $\vartheta = \frac{1}{2}\pi + \vartheta_0$. Thus a continuous solution χ_2 may be obtained from χ_1 by defining χ_2 by

$$\chi_2 = \begin{cases} \chi_1 - \exp kr\cos(\vartheta + \vartheta_0) & 0 \leq \vartheta < \frac{1}{2}\pi - \vartheta_0, \\ \chi_1 & \frac{1}{2}\pi - \vartheta_0 < \vartheta < \frac{1}{2}\pi + \vartheta_0, \\ \chi_1 - \exp kr\cos(\vartheta - \vartheta_0) & \frac{1}{2}\pi + \vartheta_0 < \vartheta. \end{cases} \quad (14)$$

Furthermore

$\chi_2 = -\exp(kr\cos\vartheta_0)$ on $\vartheta = 0$ and $\chi_2 = -\exp[kr\cos(\alpha - \vartheta_0)]$ on $\vartheta = \alpha$.

It thus appears that a solution to the diffraction problem could be obtained if χ_1 were re-written in a form valid for purely imaginary k. From (13) and (14) by a method similar to that used in deriving (10) and (11) we obtain

$$\chi = F(r, \pi - \vartheta - \vartheta_0) - F(r, \pi + \vartheta_0 - \vartheta) + \\ + F(r, \pi + \vartheta + \vartheta_0) - F(r, \pi + \vartheta - \vartheta_0) + G(r, \vartheta), \quad (15)$$

where

$$F(r, \delta) = \frac{1}{2\alpha}\sin\tau\delta \int_0^\infty \frac{e^{-kr\cosh\eta}}{\cosh\tau\eta - \cos\tau\delta}\, d\eta \quad (16)$$

and

$$G(r, \vartheta) = \begin{cases} -\exp kr\cos(\vartheta + \vartheta_0) & 0 \leq \vartheta < \pi - \vartheta_0, \\ 0 & \pi - \vartheta_0 < \vartheta < \pi + \vartheta_0, \\ -\exp kr\cos(\vartheta - \vartheta_0) & \vartheta > \pi + \vartheta_0. \end{cases} \quad (17)$$

The solution to the diffraction problem may now be obtained from (15)—(17) by replacing k by ik, and the solution so obtained agrees with that of Oberhettinger [26]).

A rigorous formulation of the diffraction problem will now be examined. The solution ϕ may be written

$$\begin{matrix} \exp ikr\cos(\vartheta - \vartheta_0) - \exp ikr\cos(\vartheta + \vartheta_0) + f_1 & 0 < \vartheta < \pi - \vartheta_0, \\ \exp ikr\cos(\vartheta - \vartheta_0) + f_2 & \pi - \vartheta_0 < \vartheta < \pi + \vartheta_0, \\ f_3 & \vartheta > \pi + \vartheta_0. \end{matrix} \quad (18)$$

The functions f_1, f_2, f_3 are required to satisfy the radiation condition. Clearly appropiate integral representations for f_1, f_2, f_3 which satisfy the boundary conditions on the wedge surfaces are

$$f_1 = \int_{-\infty}^{\infty} \exp(-ikr\cosh\eta)[F_1(\eta + i\vartheta) - F_1(\eta - i\vartheta)]\mathrm{d}\eta,$$

$$f_2 = \int_{-\infty}^{\infty} \exp(-ikr\cosh\eta)[F_2(\eta + i\vartheta) - G_2(\eta - i\vartheta)]\mathrm{d}\eta,$$

$$f_3 = \int_{-\infty}^{\infty} \exp -ikr\cosh\eta[F_3(\eta + i\vartheta - i\alpha) - F_3(\eta - i\vartheta + i\alpha)]\mathrm{d}\eta.$$

The conventional methods of asymptotic expansions [27]) show that the above expressions will satisfy the radiation condition if the terms in square brackets are absolutely integrable. The function ϕ is required to be continuous everywhere and hence

$$F_1[\eta + i(\pi - \vartheta_0) - F_1[\eta - i(\pi - \vartheta_0)] - \delta(\eta) = \\ = F_2[\eta + i(\pi - \vartheta_0)] - G_2[\eta - i(\pi - \vartheta_0)],$$

$$F_1[\eta + i(\pi - \vartheta_0)] + F_1[\eta - i(\pi - \vartheta_0)] = \\ = F_2[\eta + i(\pi - \vartheta_0)] + G_2[\eta - i(\pi - \vartheta_0],$$

$$F_2[\eta + i(\pi + \vartheta_0)] - G_2[\eta - i(\pi + \vartheta_0)] + \delta(\eta) = \\ = F_3[\eta + i(\pi + \vartheta_0 - \alpha)] - F_3[\eta - i(\pi + \vartheta_0 - \alpha)],$$

$$F_2[\eta + i(\pi + \vartheta_0)] + G_2[\eta - i(\pi + \vartheta_0)] = \\ = F_3[\eta + i(\pi + \vartheta_0 - \alpha)] + F_3[\eta - i(\pi + \vartheta_0 - \alpha)].$$

The above simultaneous difference equations are soluble by transform methods as in § 2, and it is easily found that

$$-4iF_1(\eta) = \coth\tfrac{1}{2}\tau[\eta + i\pi - i\vartheta_0] - \coth\tfrac{1}{2}\tau[\eta + i(\pi + \vartheta_0)] + \\ + \coth\tfrac{1}{2}\tau[\eta + i(\vartheta_0 - \pi)] - \coth\tfrac{1}{2}\tau[\eta - i(\pi + \vartheta_0)].$$

The solution obtained agrees with that derived from (15)—(17). The above method of formulation may be applied to the boundary condition $\partial\phi/\partial\vartheta = 0$ and also to problems with impedance conditions prescribed on the wedge surfaces. The solution in all these cases splits up into the terms of geometrical optics and a diffracted term which has an integral representation similar to that of f_1, f_2, f_3. In particular if the impedance on the wedge boundaries is such that

on these boundaries $\partial\phi/\partial\vartheta\ \phi = ikZr$ where Z is independent of k, then the integrand for the diffracted field only contains k as $\exp - ikr\cosh\eta$. It will now be shown that this fact together with the form of the solution obtained by the rigorous formulation enables the solutions for diffraction by an arbitrary time-dependent plane wave to be written down immediately. For impedances of the above form we have that, for an incident plane wave, $\exp ik[ct + r\cos(\vartheta - \vartheta_0)]$ the solution ϕ is of the form

$$e^{ikct}\left\{\begin{array}{l}\text{Plane wave terms}\\ \text{of geometrical}\\ \text{optics}\end{array}\quad + \int_0^\infty e^{-ikr\cosh\eta}F(\eta,\vartheta)d\eta\right\},$$

where $\partial F/\partial k = 0$. The corresponding solution for a plane pulse $G[ct + r\cos(\vartheta - \vartheta_0)]$ with $\partial\phi/\partial\vartheta = (Zr/c)(\partial\phi/\partial t)$ on the wedge boundaries is thus given by

$$\begin{array}{l}\text{Sum of plane}\\ \text{pulse}\\ \text{terms}\end{array}\quad + \int_0^\infty G(ct - r\cosh\eta)F(\eta,\vartheta)d\eta. \qquad \{19)$$

Boundary value problems of this type have been investigated by Papadopoulos [21] using arguments of dynamic similarity. The present approach seems to be far more direct and also gives solutions for arbitrary incident pulses and not for those of step function form only. The quantity evaluated dy Papadopoulos is $\partial\phi/\partial t$, and for a unit step function the contribution to this from the integral of (19) is

$$F(\cosh^{-1} ct/r, \vartheta)H(ct - r)$$

where H is Heaviside's unit function. The contribution is thus limited to the region $ct > r$ which corresponds to the region in which the wave equation, re-written in terms of the variables (r/t) and ϑ, is elliptic. For ϕ or $\partial\phi/\partial\vartheta$ zero on the wedges the solution (19) has been given by Friedlander [28].

It is of interest to note that these solutions of the wave equation could have been obtained directly without recourse to Fourier superposition. The time-dependent diffraction problem could have been formulated as in (19) with the functions f_1, f_2, f_3 having representations of the form

$$\int_{-\infty}^{\infty} G(ct - r\cosh\eta)[F_1(\eta + i\vartheta) + F_2(\eta - i\vartheta)d\eta.$$

The whole analysis would then proceed as before. This approach seems to yield a more general method to the solution of time-dependent diffraction problems than arguments employing dynamic similarity or the conical flows method of Keller and Blank [22]). The method seems much simpler in that a direct solution of the difference equations is obtained, and it is unnecessary to 'spot' analytic functions possessing appropriate singularities.

Received 14th July, 1960.

REFERENCES

1) Sommerfeld, A., Math. Ann. **71** (1896) 317.
2) Carslaw, H. S., Proc. Lond. Math. Soc. **18** (1920) 291.
3) Macdonald, H. M., Ibid **14** (1916) 410.
4) Kontorovich, Lebedev, J. Phys. Moscow **1** (1939) 229.
5) Oberhettinger, F., Comm. Pure Appl. Math. **7** (1954) 551.
6) Williams, W. E., Proc. Roy. Soc. A **252** (1959) 376.
7) Williams, W. E., To be published Quars. J. Mech. Appl. Math. 1960.
8) Senior, T. B. A., Comm. Pure Appl. Math. **12** (1959) 337.
9) Maliuzhinets, G. D., Thesis Phys. Inst. Acad. Sci. U.S.S.R. 1950.
10) Maliuzhinets, G. D., Soviet. Physics. Acoustics **1** (1955) 152.
11) Hasimoto, H., J. Phys. Soc. Japan **6** (1951) 400.
12) Sowerby, L., Phil. Mag. **42** (1951) 176.
13) Sowerby, L. and J. C. Cooke, Quart. J. Mech. Appl. Math. **6** (1953) 50.
14) Jaeger, J. C., Phil. Mag. **33** (1943) 527.
15) Levine, H., Appl. Sci. Res. B. **8** (1960) 105.
16) Lauwerier, H. A., Report. T.N. 16 Math. Centre, Amsterdam 1960.
17) Dantzig, D. van, Kon. Ned. Akad. Wet. A **61** (1959) 384.
18) Schwartz, L., Théorie des distributions, Vols 1 and 2, Hermaim et Cie, Paris 1950-51.
19) Lighthill, M. J., Fourier Analysis and Generalised Functions. C.U.P. 1958.
20) Carrier, G. and H. M. Munk, Proc. Symp. Appl. Math. **5** (1952) 89.
21) Papadopoulos, V. M., Proc. Roy. Soc. A **255** (1960) 538.
22) Keller, J. B. and A. Blank, Comm. Pure Appl. Math. **4** (1951) 75.
23) Papadopoulos, V. M., Proc. Roy. Soc. A **252** (1959) 520.
24) Peters, A. S., Comm. Pure Appl. Math. **5** (1952) 87.
25) Peters, A. S. and J. Stoker, Ibid **7** (1952) 565.
26) Oberhettinger, F., J. Math. Phys. **34** (1955) 245.
27) Erdelyi, A., Asymptotic Expansions, Dover 1956.
28) Friedlander, F. G., Sound Pulses, Camb. Univ. Press 1958.

ESTIMATING THE ELECTRIC FIELD INSIDE A RECTANGULAR TANK WITH BOUNDARIES AT ZERO POTENTIAL

by S. J. VELLENGA

Bataafse Internationale Petroleum Maatschappij, the Hague, Netherlands

Summary

The maximum field strength occurring in a tank of rectangular shape whose boundaries are at zero potential and which is partially filled with a liquid bearing a constant charge density can be quickly calculated by means of a strongly convergent series derived in the article. Restrictive assumptions are: 1. The charge is homogeneously distributed, 2. The difference in the values of the dielectric constant of the vapour and the liquid is ignored, 3. The surface of the liquid is parallel to the bottom of the tank.

List of symbols

a, b, c	length, width and height of the tank, respectively (m)
i	electric current entering the tank (A)
l, m, n	summation indices
p^2	$\beta^2 m^2 + n^2$
q	sV = total charge in the liquid (C)
s	charge density (C/m^3)
t	time
w	fraction of the tank's height filled
A_n	coefficient in the series for E
D	dielectric displacement (C/m^2)
E	field strength (V/m)
U	potential (V)
α	c/a
β	c/b } shape parameters
γ	fraction of the tank's height at which the field is measured
ε	relative dielectric constant
ε_0	absolute dielectric constant $8.854 \times 10^{-12}\ As/Vm$
η	$a/b = b/c$; shape parameter
τ	relaxation time (s)

§ 1. *Introduction.* The problem discussed in this article was prompted by the author's interest in the phenomenon of static electricity as it occurs in the oil industry. The underlying equation (Poisson's equation) occurs in other fields of science and therefore the derivation given below may be of interest to others as well.

Pumping a hydrocarbon liquid through a pipe or a filter often causes the liquid to become electrically charged. If such a charged liquid passes into a tank, the electric field associated with the charge will become noticeable and may increase sufficiently in strength to cause an electric spark discharge. As this presents a fire risk, it is desirable to be able to predict the magnitude and distribution of such an electric field.

For a tank of given shape the electric field is determined by the amount and distribution of charge in the liquid and by the size of the tank, but the shape of the tank also greatly influences the field strength. The present article discusses the effect of the dimensions of a partially filled rectangular tank on the electric field inside such a tank. The simplifying assumptions are:

a. the boundaries of the tank are at a constant potential,
b. the charge is homogeneously distributed,
c. the difference in dielectric constant between vapour and liquid can be ignored,
d. the surface of the liquid is parallel to the tank's bottom.

In practice nearly all tanks are made of metal, and condition *a* is therefore usually fulfilled. A homogeneous distribution of charge, while less common, may exist in tanks which are being filled at high speed, and fortunately this is a case of great practical interest from the point of view of safety. Condition *c* is of course never realized in practice, but since the dielectric constants of vapour and a hydrocarbon liquid differ only by a factor of about 2, the approximation implied by condition *c* is not very severe.

Of course, if the tank is nearly full, the field strength in the liquid will no longer be affected very much by the dielectric constant of the vapour. Since the field strength remains finite, the surface of the liquid when about to touch the roof will be equipotential with roof and walls. Consequently the field in the liquid is not influenced by the presence of the thin air gap at the top. In the absence of surface charges the dielectric displacement is continuous across the liquid surface so that the field strength in the air gap is proportional

to the field strength in the liquid at the surface, in inverse ratio to the dielectric constants.

The statement of the problem in the above form was first given by W. E. Matheson and co-workers in an internal report of the Douglas Aircraft Company Inc. (see [1])). On the basis of their work the present article gives a rapid method for the calculation of the maximum value of the field strength in a tank as described above.

§ 2. *Tanks of large lateral dimensions.* The electrical situation in a tank whose height is small in comparison with its lateral dimensions can be compared to that occurring between two infinitely extended flat plates, separated by a layer of charged liquid and a layer of vapour.

This case has been fully treated in reference [2]), p. 104, where it is shown that allowance can be made for the difference in dielectric constant between liquid and vapour by means of a correction factor. As a first approximation this correction factor can of course be applied to the equation for the field strength derived below (equation (2)), particularly if the level of the liquid is very close to the top of the tank.

In that case the situation in the tank far from the walls approaches that between two infinitely extended flat plates. Finally, it is also shown in [2]) that there may be an additional charge on the surface of the liquid. However, as this surface charge is not so likely to develop in the well-stirred tanks considered here, it will be ignored.

The relationship between the field strength E and the height c of the tank is the following:

$$E = \tfrac{1}{2} \frac{scw^2}{\varepsilon\varepsilon_0}, \qquad (1)$$

where

s = space charge density,
w = fraction of the height to which the tank is filled,
ε = relative dielectric constant of the liquid and the vapour,
ε_0 = absolute dielectric constant of vacuum.

The notation differs slightly from that of [2]).

§ 3. *General treatment.* If the lateral dimensions of the tank are not very large with respect to its height, allowance must be made for

them. This usually involves considerable computation, but for the special case considered here the arithmetic can be reduced appreciably.

For a completely full rectangular tank, with boundaries at zero potential and a homogeneous charge distribution, the potential field found by the method of Green's functions is the same as the temperature distribution in a rectangular solid with a uniform distribution of heat sources and the surface kept at zero temperature. This field is given in [3], page 1259. W. E. Matheson has extended the result to the case of partially filled tanks (see [1]).

Both [1] and [3] give the potential distribution in the form of a triple summation, each summation extending to infinity. This form is of course not very convenient for assessing a given situation. In [1] the difficulty is met by considering only the vertical field strength in the centre line of the tank, where it is larger than anywhere else. It is further assumed that the width of the tank is the geometric mean between its length and its height. By this means one shape parameter is removed from the complete equation. For a number of values of the remaining parameter the triple summation was performed over 729 terms, using an IBM 701 computer. It thus became possible to plot the field strength against a dimensionless number characterizing the liquid.

The field strength in the vertical centre line of a tank can, however, also be represented as a single series which converges rapidly, provided the height of the tank is not too much larger than its lateral dimensions. In this equation both shape parameters appear, the assumption regarding the relation between width, length and height of the tank being unnecessary. This equation reads as follows:

$$E = \tfrac{1}{2}\frac{sc}{\varepsilon\varepsilon_0}\left[w^2 - \sum_1^\infty A_n(\cos \pi n w - 1)\cos \pi n \gamma\right], \qquad (2)$$

where

A_n = a numerical factor depending on the shape parameters. Values for these factors are give in the appended table and graph.

γ = the fraction of the tank's height at which the field is measured ($\gamma \geqslant w$).

The derivation is given in Appendix I.

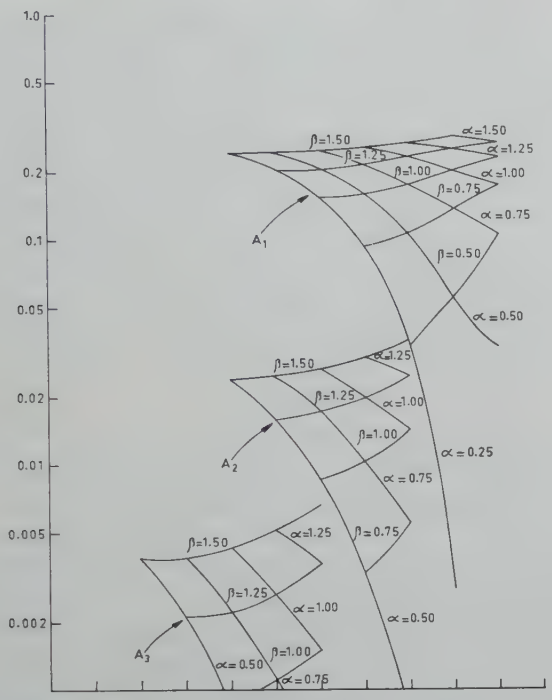

Fig. 1. Correction terms A_n in the equation for the field strength in rectangular tanks.

The main difficulty in applying (1) and (2) lies in finding a representative value for the charge density s. Ref. [2]), p. 97, gives for a full tank

$$abcs = i\tau, \tag{3}$$

where

a, b, c = length, width and height of the tank, respectively,
i = electric current entering the tank,
τ = relaxation time of the liquid.

Strictly speaking, this equation refers to an electrically stationary condition, but in practice this is approximated fairly well, because the time of filling is usually much larger than the relaxation time.

Equation (3) can also be applied if the tank is not wholly filled. If necessary, a correction might be made according to the line of thought given in [1]), p. 99.

Before (2) became available, the opportunity presented itself of testing the general approach outlined in the above by means of

some experimental data. As it was not considered to be worth while setting up a computer programme for this single case, the necessary summation of the triple series was performed with the aid of a desk calculator, and took about three days. The difference between the measured and the calculated value was only 4%. In this particular case the tank was nearly full and a correction was made for the difference in dielectric constant.

Subsequent recalculation of the field strength by means of (2) took only about half an hour; with the aid of the appended graph the calculation is only a matter of minutes.

Appendix I

Derivation of the field in a rectangular, earthed tank, containing a uniformly distributed space charge

Green's function for this case is given in [3], p. 1258. It should be noted that the numerical factor given in this reference is low by a factor of 4. Moreover, Green's function as given should be divided by a factor of $4\pi\,\varepsilon\varepsilon_0$ if a rationalized system of electrical units is used. The coordinate system used has its origin at a corner of the box. The box is thus bounded by the x, y and z-planes and the corner opposite the origin has the coordinates (a, b, c). Green's function is

$$G(\boldsymbol{r}/\boldsymbol{r}_0) = \frac{8}{\pi^2}\,\frac{s}{\varepsilon\varepsilon_0}\,\frac{1}{abc}\sum_{l,m,n}^{\infty}[(l/a)^2 + (m/b)^2 + (n/c)^2]^{-1}\,.$$

$$.\ \sin\frac{\pi l x_0}{a}\sin\frac{\pi m y_0}{b}\sin\frac{\pi n z_0}{c}\sin\frac{\pi l x}{a}\sin\frac{\pi m y}{b}\sin\frac{\pi n z}{c},$$

where $\boldsymbol{r}$ is the vector from the origin to the point (x, y, z) and the subscript 0 refers to the location of the point source.

In order to obtain the total potential distribution in the box the integration must be carried out over all charged points in the liquid volume. If the liquid level is at cw, and since we have assumed the charge density s to be constant throughout the liquid, only the following integration need be performed:

$$\int_0^a\int_0^b\int_0^{cw}\sin\frac{\pi l x_0}{a}\sin\frac{\pi m x_0}{b}\sin\frac{\pi n z_0}{c}\,\mathrm{d}x_0\mathrm{d}y_0\mathrm{d}z_0.$$

Hence the potential distribution is given by

$$U = \frac{32}{\pi^5} \frac{s}{\varepsilon\varepsilon_0} \sum_1^\infty \left[\left(\frac{l}{a}\right)^2 + \left(\frac{m}{b}\right)^2 + \left(\frac{n}{c}\right)^2\right]^{-1} \frac{(1 - \cos \pi n w)}{lmn} \cdot$$
$$\cdot \sin \frac{\pi l x}{a} \sin \frac{\pi m y}{b} \sin \frac{\pi n z}{c},$$

where the summation indices l and m only take odd values, but n takes all integer values.

Vertical field strength

The vertical field strength E_z is found by differentation

$$E_z = \partial U / \partial z.$$

The maximum value of E_z, seen as a function of x and y, occurs at $x = \frac{1}{2}a$, $y = \frac{1}{2}b$, because there $\partial E_z / \partial x = 0$ and $\partial E_z / \partial y = 0$. This maximum value of E_z is still a function of z, and in principle $\partial E_z / \partial z = 0$ should be formed in determining the location of the absolute maximum of E_z. However, it is evident physically that the maximum field strength E_z in the vapour space will occur at the liquid's surface. Since the latter value is the most interesting and can be readily computed from equations as given here, it is not necessary to write out $\partial E_z / \partial z = 0$. The maximum value of E_z, as a function of z, is now found to be

$$E_z = -\frac{32}{\pi^4} \frac{s}{\varepsilon\varepsilon_0 c} \sum_1^\infty \left[\left(\frac{l}{a}\right)^2 + \left(\frac{m}{b}\right)^2 + \left(\frac{n}{c}\right)^2\right]^{-1} \frac{(1 - \cos \pi n w)}{lm} \cdot$$
$$\cdot \sin \frac{\pi l}{2} \sin \frac{\pi m}{2} \cos \frac{\pi n z}{c},$$

where it is no longer necessary to specify odd values for the summation indices l and m because the even terms become zero in any case. This triple series can be summed with respect to each of its summation indices in turn because it is absolutely convergent; see [4]) and [5]).

The summation over l can be written as

$$\sum_1^\infty \frac{\sin l\varphi}{l(\alpha^2 l^2 + p^2)} = I,$$

where $\alpha = c/a$; $p^2 = \beta^2 m^2 + n^2$; $\beta = c/b$, whilst φ will in due course assume the value $\frac{1}{2}\pi$. Now

$$\frac{\mathrm{d}I}{\mathrm{d}\varphi} = + \frac{1}{\alpha^2} \sum_1^\infty \frac{\cos l\varphi}{l^2 + p^2/\alpha^2} =$$

$$= \frac{1}{\alpha^2} \left[\frac{\pi\alpha}{2p} \frac{\cosh(\pi - \varphi)p/\alpha}{\sinh \pi p/\alpha} - \frac{\alpha^2}{2p^2} \right].$$

For the derivation of this summation see [6]). Integrating this result,

$$I = \frac{1}{\alpha^2} \left[\frac{\pi\alpha^2}{2p^2} \left(1 - \frac{\sinh(\pi - \varphi)p/\alpha}{\sinh \pi p/\alpha} \right) - \frac{\alpha^2\varphi}{2p^2} \right],$$

where the constant of integration is found from the condition $I = 0$ for $\varphi = 0$. For $\varphi = \pi/2$

$$I = \frac{\pi}{4p^2} \left[1 - \frac{1}{\cosh(p\pi/2\alpha)} \right].$$

Substituting this result and writing $\gamma = z/c$,

$$E = - \frac{32}{\pi^4} \frac{sc}{\varepsilon\varepsilon_0} \sum_1^\infty \frac{\pi}{4m(\beta^2 m^2 + n^2)} \left[1 - \frac{1}{\cosh(p\pi/2\alpha)} \right].$$

$$.(1 - \cos \pi n w) \sin \pi m \cos \pi n \gamma.$$

The double summation can be separated into two series, one of which is

$$\sum_1^\infty \frac{\pi}{4m(\beta^2 m^2 + n^2)} (1 - \cos \pi n w) \sin \tfrac{1}{2}\pi \cos \pi n \gamma.$$

In this series the summation with respect to m can be carried out in the same way as has been done for l:

$$\frac{\pi}{4} \sum_1^\infty \frac{\sin m\varphi}{m(\beta^2 m + n^2)} = \frac{\pi^2}{16n^2} \left[1 - \frac{1}{\cosh(n\pi/2\beta)} \right].$$

Substituting this result,

$$E = - \frac{32}{\pi^4} \frac{sc}{\varepsilon\varepsilon_0} \sum_1^\infty \left[\frac{\pi^2}{16n^2} \left(1 - \frac{1}{\cosh(n\pi/2\beta)} \right) - \right.$$

$$\left. \sum_1^\infty \frac{\pi \sin m\pi/2}{4mp^2 \cosh p\pi/2\alpha} \right] (1 - \cos \pi n w) \cos \pi n \gamma.$$

The last factors can be written as a sum of cosines:

$$\cos \pi n \gamma (1 - \cos \pi n w) =$$

$$= - [\tfrac{1}{2} \cos \pi n(\gamma + w) + \tfrac{1}{2} \cos \pi n(\gamma - w) - \cos \pi n \gamma].$$

TABLE I

Coefficients A_n

$$A_n = \frac{4}{\pi^2}\frac{1}{n^2\cosh\left(\frac{n}{\beta}\frac{\pi}{2}\right)} + \frac{16}{\pi^3}\sum_1^\infty \frac{\sin(m\pi/2)}{mp^2\cosh\left(\frac{p}{\alpha}\frac{\pi}{2}\right)}$$

β \ α	0.00	0.25	0.50	0.75	1.00	1.25	1.50	∞
0.25	0.002	0.003						
0.50	0.035	0.035	0.059				$n = 1$	
0.75	0.098	0.098	0.111	0.146				
1.00	0.162	0.162	0.168	0.188	0.217			
1.25	0.213	0.213	0.216	0.228	0.246	0.266		
1.50	0.253	0.253	0.254	0.261	0.272	0.286	0.300	0.405

β \ α	0.50	0.75	1.00	1.25	1.50	∞	
0.50	0.001						
0.75	0.003	0.006					$n = 2$
1.00	0.009	0.011	0.015				
1.25	0.016	0.018	0.021	0.026			
1.50	0.025	0.026	0.029	0.032	0.037	0.101	

β \ α	0.50	0.75	1.00	1.25	1.50	∞	
0.50	0.000						$n = 3$
0.75	0.000	0.000					
1.00	0.001	0.001	0.002				
1.25	0.002	0.002	0.003	0.004			
1.50	0.004	0.004	0.004	0.005	0.007	0.045	

β \ α	1.00	1.25	1.50	∞	
1.00	0.000				
1.25	0.000	0.001			$n = 4$
1.50	0.001	0.001	0.001	0.002	

β \ α	1.25	1.50	
1.25	0.000		
1.50	0.000	0.000	$n = 5$

Now

$$\sum_1^\infty \frac{\cos n\Theta}{n^2} = \tfrac{1}{4}(\Theta^2 - 2\pi\Theta + \tfrac{2}{3}\pi^2) \text{ (see e.g. ref. [7]), p. 3).}$$

Therefore

$$\sum_1^\infty \frac{\pi^2}{16}\,\frac{\cos\pi n(\gamma + w) + \cos\pi n(\gamma - w) - 2\cos\pi n\gamma}{2n^2} = \frac{\pi^4}{64}\,w^2.$$

Substituting this result,

$$E = \frac{sc}{2\varepsilon\varepsilon_0}\left[w^2 - \frac{4}{\pi^2}\sum_1^\infty \frac{(\cos \pi n w - 1)\cos \pi n \gamma}{n^2 \cosh n\pi/2\beta} - \frac{16}{\pi^3}\sum_1^\infty\sum_1^\infty \frac{(\cos \pi n w - 1)\cos \pi n \gamma \sin m\pi/2}{mp^2 \cosh p\pi/2\alpha}\right].$$

The series in this expression usually converge extremely rapidly, so that in most cases a few terms suffice to give a reasonable approximation. Slight rearranging and numerical evaluation of certain constants lead to (2) in the main part of this report. The factors A_n can be calculated from

$$A_n = \frac{4}{\pi^2}\frac{1}{n^2 \cosh n\pi/2\beta} + \frac{16}{\pi^3}\sum \frac{\sin m\pi/2}{mp^2 \cosh p\pi/2\alpha}.$$

This series converges very rapidly indeed. For example, if $\alpha = 0.724$ and $\beta = 1.484$, the first term is 0.2510 and the second term is already extremely small: 0.00661. By double linear interpolation in table I a value of 0.258 is found.

Received 23rd July, 1960.

REFERENCES

1) Manacher, G. K., W. E. Matheson and J. W. McKee, The Development of Electric Fields in the Gas Space above the Surface of a Liquid during Filling of Grounded Boundary Rectangular Reservoirs, Internal Report of the Douglas Aircraft Company Inc., Santa Monica Division.
2) Electrostatics in the Petroleum Industry. A Royal Dutch/Shell Research and Development Report. Edited by A. Klinkenberg and J. L. van der Minne, Ed. Elsevier Publishing Co., Amsterdam 1958.
3) Morse, P. M. and H. Feshbach, Methods of Theoretical Physics, Part II. McGraw Hill, New York 1953.
4) Whittaker, E. T. and G. N. Watson, A Course of Modern Analysis, Cambridge University Press, 4th ed., 1950.
5) Bailey, W. M., Proc. Camb. Phil. Soc. **25** (1929) 410.
6) Bromwich, T. J. I'a, Theory of Infinite Series. Macmillan and Company Ltd, London 1947.
7) Erdélyi, A., W. Magnus, F. Oberhettinger and F. G. Tricomi, Higher Transcendental Functions, Vol. I. McGraw Hill, New York 1953.

LAMINAR STAGNATION FLOW OF AN ELECTRICALLY CONDUCTING FLUID AGAINST AN INFINITE PLATE IN THE PRESENCE OF A TRANSVERSE MAGNETIC FIELD

by A. S. GUPTA

Department of Applied Mathematics, Indian Institute of Technology, Kharagpur, India

Summary

The two-dimensional stagnation flow of an electrically conducting, incompressible and viscous fluid against a plane wall is investigated for the case when the induced field is negligible compared to the imposed transverse magnetic field. It is found that the component of the velocity parallel to the plate as well as the drag coefficient decrease with the increase in the magnetic field. Furthermore, it is observed that the velocity component parallel to the plate is essentially constant except in a layer of constant thickness, a result which is true in the non-magnetic case also.

§ 1. *Introduction.* The problem of two-dimensional stagnation flow of an incompressible viscous fluid against a plane wall was completely solved by Blasius [1]) and Hiemenz [2]). Blasius reduced the partial differential equations for the flow to ordinary differential equations with requisite boundary conditions, and these were integrated numerically by Hiemenz. The solution of Hiemenz was, however, improved by Howarth [3]). This exact solution has close relation to solutions of the boundary-layer type for flows past an arbitrarily shaped body and substantiates the assumptions of the boundary layer theory in the most important region of the field of flow. The present note is an extension of this problem to the case of an electrically conducting fluid in the presence of a transverse magnetic field. This solution, however, has an important bearing on missile re-entry problems. When a missile re-enters the earth's atmosphere, a sufficient amount of heat is generated due to friction of the air molecules. This viscous heating may sometimes be so

large as to ionise the air near the forward stagnation point. As ionised air is electrically conducting, a magnetic field may be applied to induce forces in the air which in turn will be retarded, the rate of heat transfer at the wall being reduced as a consequence.

§ 2. *Basic equations and their solutions.* The stagnation point in two-dimensional laminar flow against an infinite plate is taken as the origin, y is the distance from the plate and x the distance along the plate in the plane of the flow. A constant magnetic field H_0 is applied along the y-direction.

The equation of continuity is

$$\frac{\partial u}{\partial x} + \frac{\partial v}{\partial y} = 0. \tag{1}$$

The equations of momentum are

$$u\frac{\partial u}{\partial x} + v\frac{\partial u}{\partial y} = -\frac{1}{\rho}\frac{\partial p}{\partial x} + \nu\left(\frac{\partial^2 u}{\partial x^2} + \frac{\partial^2 u}{\partial y^2}\right) - \frac{\sigma B^2}{\rho}u, \tag{2}$$

$$u\frac{\partial v}{\partial x} + v\frac{\partial v}{\partial y} = -\frac{1}{\rho}\frac{\partial p}{\partial y} + \nu\left(\frac{\partial^2 v}{\partial x^2} + \frac{\partial^2 v}{\partial y^2}\right), \tag{3}$$

where σ is the electrical conductivity and $B = \mu_e H_0$, μ_e being the magnetic permeability. In writing these equations, the secondary effects of magnetic induction are ignored [4]). We have also assumed that the electric field is zero; this seems to be a justifiable assumption since no external electric field is applied and the effect of polarisation of the ionized field may be expected to be small if two-dimensional conditions occur in the ionized layer [5]). In view of these assumptions, the Maxwell equations become superfluous.

The velocity distribution in the potential flow in the neighbourhood of the stagnation point at $x = y = 0$ is given by

$$u_\infty = \beta x; \quad v_\infty = -\beta y. \tag{4}$$

Using (4), the pressure gradient $\partial p/\partial x$ is now obtained from (2) with $\nu = 0$ as

$$-\frac{1}{\rho}\frac{\partial p}{\partial x} = \beta'^2 x, \tag{5}$$

where

$$\beta'^2 = \beta^2 + \frac{\sigma B^2}{\rho}\beta. \tag{6}$$

It follows from (5) and (6) that the pressure distribution is affected by the magnetic field.

If the stream function ψ is used such that

$$u = \frac{\partial \psi}{\partial y}, \quad v = -\frac{\partial \psi}{\partial x}, \tag{7}$$

the equation of continuity is automatically satisfied. From

$$\psi = \sqrt{\nu \beta'}\, x F(\eta), \quad \eta = \sqrt{\frac{\beta'}{\nu}}\, y \tag{8}$$

if follows that

$$u = \beta' x F'(\eta), \quad v = -\sqrt{\nu \beta'}\, F(\eta). \tag{9}$$

Using (5) and (9), we have from (2)

$$F''' + FF'' = F'^2 - 1 + CF', \tag{10}$$

where

$$C = \frac{\sigma B^2}{\rho \beta'}. \tag{11}$$

The boundary conditions are

$$u = v = 0 \text{ at } y = 0; \; u = \beta x \text{ at } y = \infty. \tag{12}$$

These give from (9):

$$F(0) = 0, \; F'(0) = 0; \; F'(\infty) = \beta/\beta'. \tag{13}$$

Using (6) and (11), we have

$$\left(\frac{\beta}{\beta'}\right)^2 + C\,\frac{\beta}{\beta'} = 1,$$

and the solution (positive) of this equation is given by

$$\frac{\beta}{\beta'} = \frac{-C + \sqrt{C^2 + 4}}{2}. \tag{14}$$

Thus we have to solve (10) subject to

$$F(0) = 0, \quad F'(0) = 0, \quad F'(\infty) = \frac{-C + \sqrt{C^2 + 4}}{2}. \tag{15}$$

The equation (10) is non-linear and differs from that derived by

Blasius by the presence of the term CF' representing the influence of the magnetic field. This equation subject to (15) has been integrated with the help of the Analog Computer EASE (at the Indian Institute of Technology, Kharagpur) for three different values of C,

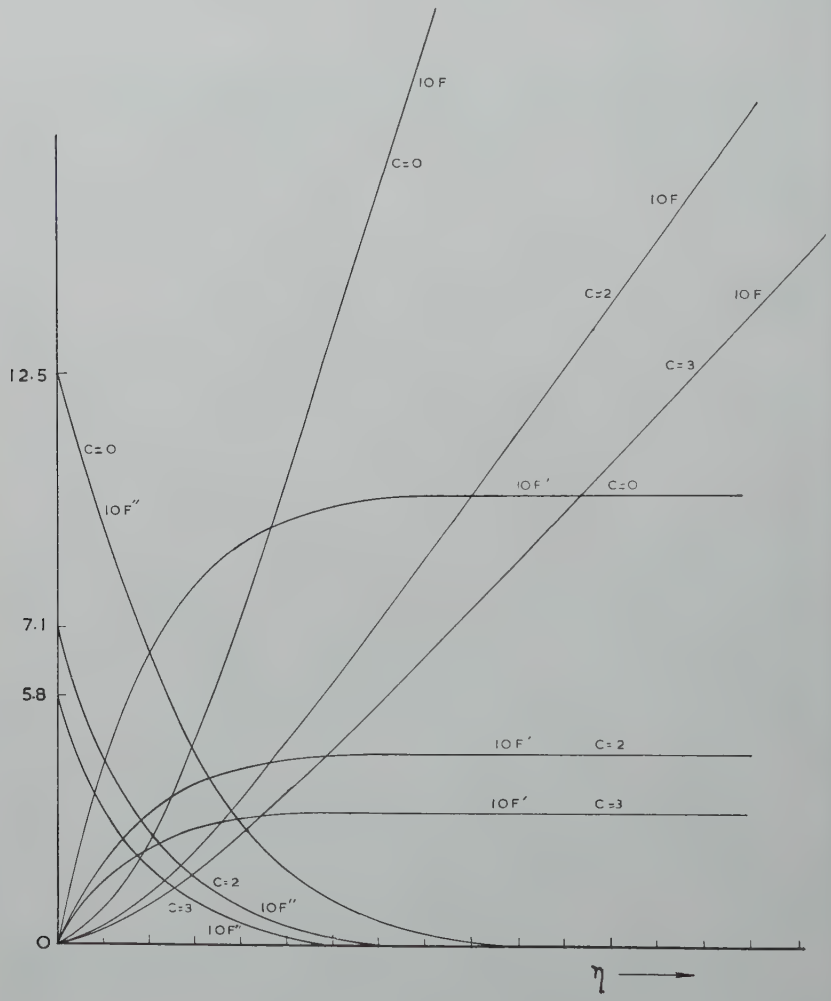

Fig. 1. Variations of F, F' and F'' with η.

viz., 0, 2 and 3. The solution for the case $C = 0$ (i.e. the non-magnetic case) shows excellent agreement with Howarth's solution. Graphs for F, F' and F'' are drawn in fig. 1 showing the influence of the magnetic field. From the graph it can be seen that

F', and hence u/x, is essentially constant except in a layer of constant thickness. The constancy of this thickness is due to the decreasing pressure along the plate in the direction of flow, which compensates for its normal growth due to viscosity. It is also seen that F' decreases with the increase in the magnetic field.

Using (9) the skin-friction

$$\tau_\omega = \left(\mu \frac{\partial u}{\partial y}\right)_{y=0}$$

at a station x is given by

$$\frac{\sqrt{\nu}\,\tau_\omega}{x\mu\beta'^{3/2}} = F''(0). \tag{16}$$

The values of $F''(0)$ for $C = 0$, 2 and 3 (as read from the graph) are shown in table I.

TABLE I

C	$F''(0)$
0	1.25
2	0.71
3	0.58

This shows that the effect of an increase in the magnetic field is to decrease the drag-coefficient.

Again, from (9) the second equation of motion (3) becomes

$$v \frac{\partial v}{\partial y} = -\frac{1}{\rho} \cdot \frac{\partial p}{\partial y} + \nu \frac{\partial^2 v}{\partial y^2},$$

which can be integrated to give

$$\frac{p}{\rho} = \phi(x) - \tfrac{1}{2}v^2 + \nu \frac{\partial v}{\partial y}, \tag{17}$$

where $\phi(x)$ is an arbitrary function. Using (5), the above equation gives

$$\phi'(x) = -\beta'^2 x.$$

Thus (17) becomes

$$\frac{p}{\rho} = C - \frac{\beta'^2 x^2}{2} - \tfrac{1}{2}v^2 + \nu \frac{\partial v}{\partial y},$$

which by virtue of (9) becomes

$$\frac{p}{\rho} = C - \frac{\beta'^2 x^2}{2} - \frac{\nu\beta'}{2} F^2(\eta) - \nu\beta' F'(\eta). \tag{18}$$

Since $F(\eta)$ and $F'(\eta)$ are known from the graph, the pressure distribution at a station x is known from (18).

In conclusion I express my sincere thanks to Mr. A. K. Chaudhuri for his kind help in the solution of the differential equation with the analog computer.

Received 5th July, 1960.

REFERENCES

1) Blasius, H., Advanced Mechanics of Fluids, edited by H. Rouse, John Wiley, p. 232.
2) Hiemenz, K., Dingl. Polytech. J. **326** (1911) 321.
3) Howarth, L., ARC Rep. and Memo. 1935, p. 1632.
4) Rossow, V. J., NACA Report 1957, TN 3971.
5) Resler, E. L. and W. R. Sears, J. Aero. Sci. **25** (1958) 235.

COMPLEX CONDUCTIVITY OF SOME PLASMAS AND SEMICONDUCTORS

by P. H. FANG *)

National Bureau of Standards, Washington, D.C., U.S.A.

Summary

The complex conductivities of plasmas and semiconductors have been calculated for several cases where the collision frequency can be expressed as a power function of the energy. From the result, some characteristic parameters of the plasma originally investigated by Spitzer are estimated. The problem of determining the relaxation time from a non-symmetrical dispersion is discussed.

§ 1. *Introduction.* The nature of the electrical conductivity of weakly ionized gases and of some semiconductors is determined by the scattering processes. It is possible to express the effect of the scattering in terms of a relaxation time (or a collision frequency). Theoretically, the frequency spectrum of the a.c. conductivity can be derived from the energy dependence of the relaxation time [1)2)]. Hence, in principle, an experimental determination of the frequency spectrum should be capable of revealing the scattering mechanisms. Because of the presence of certain complicated integrals in the mathematical formulation, most of the theoretical discussions have been restricted to qualitative or asymptotic behaviour of the conductivity at extremely high or low frequencies. Consequently, the applicability of the theory in analyzing experimental results has not been thoroughly investigated. In this paper the frequency spectra of the conductivity of several different kinds of gaseous plasmas, as well as conductivity due to various scattering mechanisms in semiconductors, will be calculated. From the results we will establish certain quantitative relations between the dispersion quantities and the energy dependence of the collision

*) At present at the Institut Fourier, Grenoble, France.

frequency or the relaxtion time. Through interpolation we will also discuss the a.c. conductivities of the plasmas investigated by Cohen, Spitzer and Rotly, and by Spitzer and Harm [3].

§ 2. *Mathematical formulation.* The complex conductivity, σ^*, when the energy distribution is Maxwellian, can, in general, be expressed as follows [1]:

$$\sigma^*(\omega) = \frac{4e^2n}{3\sqrt{\pi}\, m} \int \frac{\varepsilon^{3/2} e^{-\varepsilon}}{\nu + i\omega} \, d\varepsilon, \tag{1}$$

where n is the number density of electrons, m and e are the mass and the charge of the electron, respectively, ω is the frequency of the applied field, ν is the collision frequency of electrons, and $\varepsilon = mv^2/2kT$ where v, in the case of ionized plasma, is the relative velocity of electrons with respect to ions or molecules. The integration limits here, and throughout this paper, are always from 0 to ∞ for the corresponding integration variable.

In the case of semiconductors, the relaxation time, which is the reciprocal of the collision frequency, is more frequently used because of the usual quantum mechanical formalism. The expression is now [2]

$$\sigma^*(\omega) = \frac{4e^2n}{3\sqrt{\pi}\, m^*} \int \frac{\tau\varepsilon^{3/2} e^{-\varepsilon}}{1 + i\omega\tau} \, d\varepsilon, \tag{2}$$

where m in (1) becomes m^*, the effective mass of the electron. The relative velocity which is related to ε is now the relative velocity of the electrons with respect to the lattices or impurity centres.

TABLE I

Classification of Plasmas and Semiconductors according to p values

p	Plasmas	Semiconductors
− 5/2 *)		ref. [8]
− 2 *)		ref. [8]
− 3/2	ref. [3]	refs. [2a, 4]
− 1	ref. [4], H_2O, NH_3	
− 1/2		ref. [9]
0	Lorentz	Lorentz
1/2	ref. [5], He	ref. [2a], p. 235
1	ref. [6], air, ref. [1a, 7], N_2	
3/2		

*) The calculations were not made in these cases. See however table II.

On the basis of experimental or theoretical results, various authors (see table I) have suggested the following relation between ν and ε:

$$\nu = a_p{}^{-1}\varepsilon^p \tag{3}$$

or, equivalently,

$$\tau = a_p\varepsilon^{-p}, \tag{4}$$

where the coefficient a_p is independent of ε, but may depend on the temperature. These relations are obtained either as asymptotic forms from the theory or, in the case of experiment, as approximations over a finite energy range. In the integration, however, the Maxwellian factor $\varepsilon^{3/2}e^{-\varepsilon}$ converges strongly at large values of ε. At small values of ε, the factor converges as the 3/2-th power of ε. Therefore, the exact form of ν is not important as long as ν does not diverge more strongly than the $(-3/2)$-th power of ε as ε approaches zero. This point will be discussed further in § 6. Table I lists the values of p which correspond to plasmas of different gases and to semiconductors. In the case of semiconductors, specific scattering mechanisms have not been identified because several different mechanisms could lead to the same value of p. For the actual applications, therefore, the references should be consulted. The case corresponding to $p = 0$, which leads to Lorentzian dispersion, is well known, and the numerical evaluation is elementary. Two other cases, i.e., $p = \pm \frac{1}{2}$, have been previously calculated [10]). Also included in the table are cases of several values of p which we cannot now relate to physical processes but these results might be useful in the analysis of the experimental results in study of plasmas and semiconductors.

§ 3. *Numerical evaluations.* The numerical evaluation of the integrals of (1) or (2) is very simple when certain functions introduced by Dingle et al. [11]) are used. These functions are:

$$\mathfrak{A}_p(x) = (p!)^{-1}\int \frac{\varepsilon^p e^{-\varepsilon}}{\varepsilon + x}\,d\varepsilon, \tag{5a}$$

$$\mathfrak{C}_p(x) = (p!)^{-1}\int \frac{\varepsilon^p e^{-\varepsilon}}{\varepsilon^2 + x^2}\,d\varepsilon, \tag{5b}$$

$$\mathfrak{E}_p(x) = (p!)^{-1}\int \frac{\varepsilon^p e^{-\varepsilon}}{1 + x\varepsilon^3}\,d\varepsilon. \tag{5c}$$

Substituting the relation of (3) into (1),

$$\sigma^* = Ka_p \int \frac{(\varepsilon^p - ix_p)}{\varepsilon^{2p} + x_p{}^2} \varepsilon^{3/2} e^{-\varepsilon} d\varepsilon, \tag{6}$$

where $K = 4e^2n/3\sqrt{\pi m}$, $x_p = a_p\omega$. The integral of (6) may be represented by one of the functions of (5), (see Appendix 1). Numerical values may then be obtained from the tables of these functions by simple multiplication. In the extreme frequency ranges where the functions are not covered by the numerical tables, asymptotic forms, also given by Dingle, can be used. These forms may be simplified for special values of p (see Appendix 1). The numerical values themselves are not listed since the calculations involved are straightforward.

§ 4. *Analysis.* The usual method of analyzing the frequency spectrum of a relaxation dispersion is to plot σ' and σ'', the real and imaginary parts of σ^*, in the log ω-space and to discuss the characteristics of the curves in this space. Fig. 1 shows the frequency

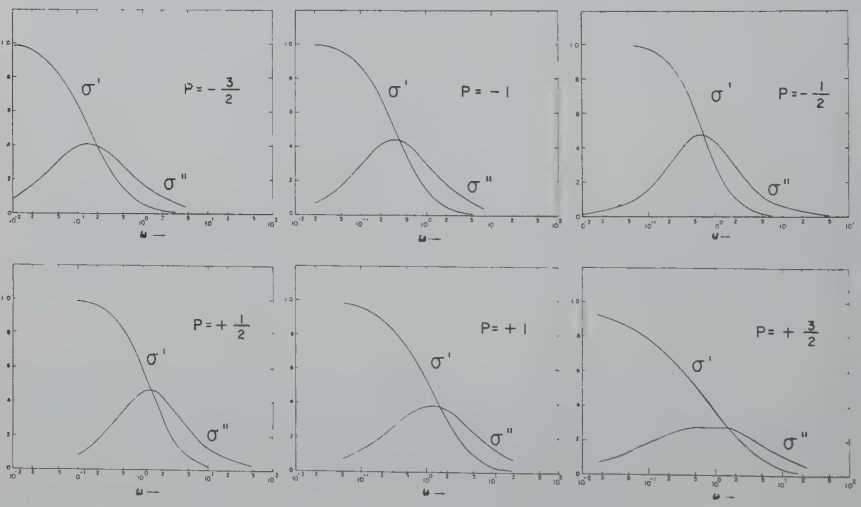

Fig. 1. The frequency spectra of σ' and σ''.

spectra for various values of p in this representation. The half width, Γ, and the maximum value of σ'' as a function of p are shown in fig. 2. The half width shows a minimum where $p = 0$, and increases when the absolute value of p increases. Obviously, the two para-

meters Γ and σ_{max}'' alone are not sufficient to describe completely the line shape. For a comparatively more precise description, we introduced previously an Argand diagram [10]). This diagram is the frequency trace in the complex plane of σ^*. We have shown that when $p = 0$, the trace of the diagram is a semi-circle. When $p = \pm \frac{1}{2}$ the trace is approximately identical to the so-called Cole-Cole (abbreviated as C–C hereafter) arc [12]). This arc is a

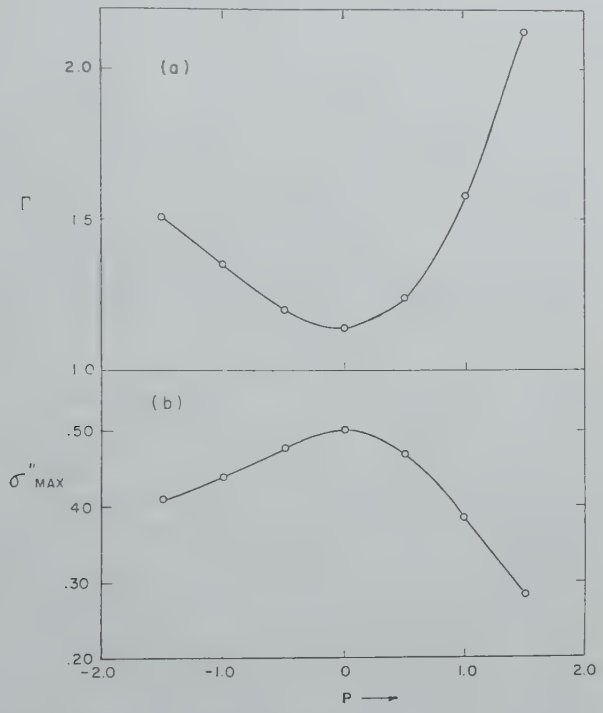

Fig. 2. The half width Γ and the maximum of σ'' for different values of p.

semicircle with the center depressed from the σ'-axis by an angle $\theta = \pi/2(1 - \alpha)$, where α lies between 0 and 1. When the absolute value of p becomes larger than $\pm \frac{1}{2}$, the arc approximation becomes poorer. Nevertheless if we draw arcs passing through the end points and the maximum point of the numerically calculated curves, these arcs provide a method for the description of dispersion data. When p is positive, the deviation from the C–C arc is greatest in the region of moderately high frequencies; it is greatest in the moderately

low-frequency region when p is negative. These diagrams are illustrated in fig. 3. Fig. 4 shows the dependence of θ on p.

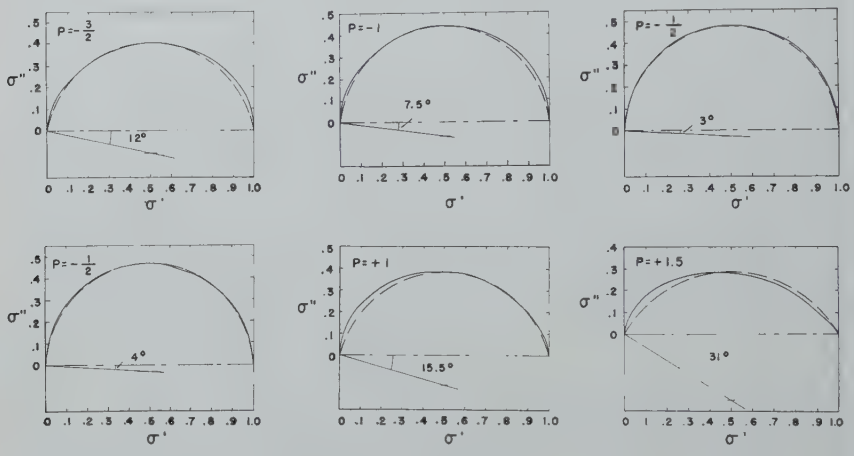

Fig. 3. Argand diagram of the complex conductivity: solid line, calculated from (6), dotted line. Cole and Cole arc approximation.

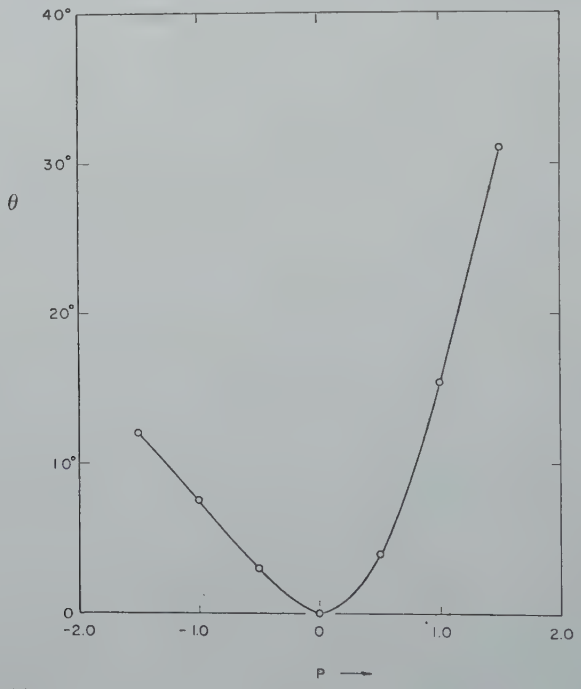

Fig. 4. The angle of Cole and Cole arc, θ, for different values of p.

The above description must be modified for extreme frequencies where σ'' approaches zero. In the case of the arc given by (6), the tangents of the arc at $\omega = 0$ and $\omega \to \infty$ make $\pm 90°$ intersections with σ'-axis (see Appendix 2). On the other hand, the tangents of the C–C arc make angles of $\pm \pi/2(1 - \alpha)$. This difference will become important when considering the pressure dependence of the conductivity [1c]), or the frequency dependence of the dissipation term in the Langevin equation [1d]). The terms in question diverge to infinity at infinite pressure or infinite frequency, respectively, for the C–C form of dispersion, while finite for the dispersion of (6).

§ 5. *Fully ionized plasma.* Spitzer's investigation of a fully ionized plasma has been much discussed. More recently, Sodha and Varshni [13]) have given a simple approximation to replace Spitzer's complicated relation for the relaxation time and the energy of the electrons. This approximation is for the case of the mean ionic charge $Z = 1$ and can be written as

$$\tau = B\varepsilon^{0.722}, \tag{7}$$

where B is a constant dependent on the impurity concentration. We have not explicitly calculated σ^* for this case because σ^* cannot simply be expressed in terms of known functions. However, it can be shown that, in general, σ^* is a continuous, non-singular function of p. Therefore, one can obtain the characteristic parameter of the complex conductivity by interpolation. The results are:

$$\begin{aligned} &\sigma''_{\max} = 0.420 \text{ corresponding to } \tau = 0.810\varepsilon^{0.722}, \\ &\theta = 8.4°, \\ &\Gamma = 1.38 \text{ logarithmic cycle.} \end{aligned} \tag{8}$$

The deviation of the arc in the Argand diagram from the C–C arc will be appreciable in the high frequency region.

Spitzer has given the following relation for the case in which the ionic charge approaches infinity:

$$\tau = B\varepsilon^{1.5}. \tag{9}$$

The complex conductivity in this case has already been given in our discussion for $p = -1.5$.

§ 6. *Relaxation time.* In this section the relaxation time according to the usual formalism of relaxation theory will be discussed. A

dispersion quantity $Q^*(\omega)$ can be represented, in general, by the following integral [14]),

$$Q^*(\omega) = [Q(0) - Q(\infty)]N \int \frac{g(\tau)}{1 + i\omega\tau} \, d\tau, \tag{10}$$

where $g(\tau)$ is the distribution function of relaxation times, and N is a normalization constant such that

$$N \int g(\tau) d\tau = 1. \tag{11}$$

A similar formalism can be introduced in the investigation of the dispersion of the conductivity of plasmas or semiconductors [10]). Instead of $d\tau$ in (9) or (10), sometimes $d \log \tau$ has been used in the integration in the literature of dielectric relaxation theory [12]). This difference has been considered purely as conventional and in our earlier investigation [10]), a formulation similar to that of (10) has been adapted. A unique formulation is provided by the dimension of Q and g, and the requirement that the distribution function should be normalizable independent of the parameter p of (4) [15]). In this way, a distribution function of relaxation times, $g(\tau)$, is defined in the following manner [16]):

$$\sigma^*(\omega) = KN \int \frac{\tau g(\tau)}{1 + i\omega\tau} \, d \log \tau. \tag{12}$$

Two applications of this relaxation time formulation are: *i*) since the distribution function $g(\tau)$ is the Stieltjes' transform of $\sigma^*(\omega)$, one can determine the distribution characteristics of relaxation times from the frequency dispersion data; and ii) from $g(\tau)$, the average value of τ or ν can be evaluated. For the first application, in the present paper, we will only discuss the determination of a relaxation time parameter because the problem to find $g(\tau)$ through the inverse transform is not required: $g(\tau)$ is already given by (1), namely,

$$g(\tau) = \frac{1}{|p|} \left(\frac{a_p}{\tau}\right)^{\frac{1}{2}p} \exp\left[-\left(\frac{a_p}{\tau}\right)^{1/p}\right], \tag{13}$$

where (4) has been used, $|p|$ stands for the absolute value of p. This additional notation, $|p|$, is used in order that the integration limits will always be taken from 0 to ∞. A relaxation time parameter τ_0 which corresponds to the most probable value of τ, is obtained by maximizing $g(\tau)$ with respect to $\log \tau$,

$$\tau_0 = (\tfrac{2}{5})^p a_p. \tag{14}$$

Now, experimentally, the relaxation time is usually determined from the reciprocal of the frequency corresponding to either the maximum of $\sigma''(\omega)$, or the inflection point of $\sigma'(\omega)$. Denote the relaxation times determined in this way by τ_1 and τ_2, respectively. It can be shown [17]) that the value of τ_0 is identical to that of τ_1 or τ_2 *if and only if* $g(\tau)$ is a symmetrical dispersion function, in the following sense:

$$g(\tau/\tau_0) = g(\tau_0/\tau). \tag{15}$$

The distribution function of the present problem, which was given by (13), does not satisfy (15); therefore, τ_0 is not equal to τ_1 or τ_2. Table II lists the numerical values of τ_0, τ_1, and τ_2 for different values of p.

The distribution function $g(\tau)$, as given by (13) has all the requirements of a distribution function, namely: (i), $g(\tau)$ is a non-negative everywhere, (ii) it can be normalized, with a normalization factor determined from (13) and (15):

$$N = \tfrac{3}{4}\sqrt{\pi}, \tag{16}$$

and (iii), $g(\tau)$ is zero both when τ is at zero or infinity. All of the above characteristics of $g(\tau)$ are independent of the value of sign of p. In spite of this satisfactory behaviour, we observe that for certain values of p the mean value (first moment) of τ or ν does not exist. The mean value of τ, denoted by $\langle\tau\rangle_g$, is defined by [18]),

$$\langle\tau\rangle_g = \int \tau g(\tau) \mathrm{d}\log\tau \Big/ \int g(\tau)\mathrm{d}\log\tau = \frac{4}{3\sqrt{\pi}}\, a_p \int \varepsilon^{\frac{1}{2}-p}\, \mathrm{e}^{-\varepsilon}\, \mathrm{d}\varepsilon. \tag{17}$$

The pathological nature of $\langle\tau\rangle_g$ is obvious when one compares (17) with the Gamma-function integral and recalls that when $\frac{3}{2} - p \leq -1$, the integral is not defined. One can apply an analytic continuation and define this integral in the sense of the Cauchy residue theorem, but the resultant $\langle\tau\rangle_g$ has negative or infinite values for some $p \geq 5/2$. Therefore, the first moment of τ remains unphysical.

Molmud [1d]) has discussed a mean value of ν, $\langle\nu\rangle_M$, which is defined as an average over the Maxwellian distribution; in the present notation,

$$\langle\nu\rangle_M = \frac{2}{\sqrt{\pi}} \int \nu\varepsilon^{\frac{1}{2}}\, \mathrm{e}^{-\varepsilon}\, \mathrm{d}\varepsilon, \tag{18}$$

a similar pathological problem as that of $\langle\tau\rangle_g$ arises when $p \leq -\frac{3}{2}$.

The above discussion is dependent on the value of p. Now, p is dictated by the physical result, but otherwise arbitrary from the point of view of general mathematical formalism. Therefore, for some large values of the absolute values of p, the concept of the mean value of τ or ν is not meaningful in the present problem [19].

As a numerical summary, a list of values of the various relaxation times as defined above and corresponding to different values of p is compiled in table II.

TABLE II

Relaxation times calculated from different definitions					
p	τ_0/a_p	$\omega^2\tau^2$	$\omega_2\tau_2$	$\langle\tau\rangle_g/a_p$	$1/\langle\nu\rangle_M a_p$
− 1.5	3.95	6.67	7.09	4.52	0
− 1	2.50	3.08	3.00	2.50	0.50
− 0.5	1.58	1.60	1.60	1.51	0.89
0	1.00	1.00	1.00	1.00	1.00
0.5	0.63	0.81	0.76	0.75	0.89
1	0.40	0.88	0.83	0.67	0.67
1.5	0.25	1.83	1.34	0.75	0.44
2	0.16	—	—	1.33	0.27
2.5	0.10	—	—	∞	0.07

§ 7. *Conclusion.* The complex conductivities of plasmas and semiconductors have been calculated in cases where the collision frequency can be expressed as a power function of the energy. From the results, we have established several numerical relations between the nature of the collision frequency and the characteristics of the dispersion functions. As an application of the results, we have estimated some characteristic parameters of the plasmas originally investigated by Spitzer.

The problem of the determination of the relaxation time parameter for the dispersion with non-symmetrical distribution of relaxation times, as well as the nature of the average relaxation time and the average collision frequency are discussed.

The present mathematical procedure and the numerical results can be trivially extended to the calculation of the mobility in semiconductors due to the magnetic field, and to galvanomagnetic effects [20] in general.

Appendix 1

In the following, the complex conductivity will be expressed in terms of special functions of Dingle et al. The asymptotic forms of these functions will also be listed. σ^* will be expressed in the form:

$$\sigma^* = KAa_p(\sigma' - i\sigma'').$$

The coefficient A, which depends on p, will be chosen such that $\sigma' = 1$ at the zero frequency. To avoid cumbersome subscripts in the discussion under special values of p, the subscript of x will be omitted. Also, the reciprocal of x will be denoted by y to further simplify the mathematical expressions.

a) $p = -\frac{3}{2}$:

$$A = 3!, \quad \sigma' = \mathfrak{F}_3(x^2), \quad \sigma'' = \frac{4.5!}{3!} \times \mathfrak{F}_{4.5}(x^2).$$

When x is very small,

$$\mathfrak{F}_3(x^2) = 1 - 120x + 6.048 \times 10^4 x^2,$$

$$\mathfrak{F}_{4.5}(x^2) = 1 - 268x + 2.273 \times 10^5 x^2.$$

When x is very large, we will expand $\mathfrak{F}_p$ in terms of y

$$\mathfrak{F}_3(x^2) = y[0.167 - 0.201(y^{\frac{1}{3}} - y^{\frac{2}{3}}) + 0.004y - 0.018y \log y],$$

$$\mathfrak{F}_{4.5}(x^2) = 0.025y(1 - 2.67y) - 0.0113y^{11/6}\exp(y^{\frac{2}{3}}) \left[1 - 2\exp(-\tfrac{3}{2}y^{\frac{1}{3}}) \cos\left(\frac{\pi}{3} - \frac{\sqrt{3}}{2}y^{\frac{1}{3}}\right)\right].$$

b) $p = -1$:

$$A = 2.5!, \quad \sigma' = y^2\mathfrak{C}_{2.5}(y), \quad \sigma'' = \tfrac{7}{2}y\mathfrak{C}_{3.5}(y).$$

For small values of y,

$$\mathfrak{C}_{2.5}(y) = \tfrac{1}{3.75}(1 + 4y^2) - 0.945y^{1.5}\sin(0.785 + y),$$

$$\mathfrak{C}_{4.5}(y) = \tfrac{1}{8.75}(1 - 0.335y^2) - 0.220y^{2.5}\cos(0.785 + y).$$

For large values of y,

$$\mathfrak{C}_{2.5}(y=) \; x^2(1 - 15.75x^2),$$

$$\mathfrak{C}_{3.5}(y) = x^2(1 - 24.75x^2).$$

c) $p = -\frac{1}{2}$:

$$A = 2,\ \sigma' = y^2\mathfrak{A}_2(y^2),\ \sigma'' = \tfrac{3!}{2}\, y\mathfrak{A}_{2.5}(y^2).$$

For small values of y,

$$\mathfrak{A}_{2.5}(y^2) = \tfrac{1}{2.5}\,(1 - 0.667y^2 + 1.333y^4) - 0.947y^5 \exp(y^2),$$
$$\mathfrak{A}_2(y^2) = \tfrac{1}{2}(1 - y^2) - y^4 - (0.577 + 2\log y)(1 - y^4).$$

For large values of y,

$$\mathfrak{A}_2(y^2) = x^2(1 - 3x^2 + 12x^4),$$
$$\mathfrak{A}_{2.5}(y^2) = x^2(1 - 3.5x^2 + 15.75x^4).$$

d) $p = 0$:

$$A = 1.5!,\quad \sigma' = 1/(1 + x^2),\quad \sigma'' = x/(1 + x^2).$$

e) $p = +\frac{1}{2}$:

$$A = 1,\quad \sigma' = 2\mathfrak{A}_2(x^2),\quad \sigma'' = (1.5!)x\mathfrak{A}_{1.5}(x^2).$$

The asymptotic form of $\mathfrak{A}_2(x^2)$ was given in *c*). For $\mathfrak{A}_{1.5}(x^2)$, when x is small

$$\mathfrak{A}_{1.5}(x^2) = \tfrac{1}{1.5}\,(1 - 2x^2 - 4x^4) + 1.965x^3 \exp(x^2);$$

when x is large

$$\mathfrak{A}_{1.5}(x^2) = y^2(1 - 2.5y^2 + 8.75y^4).$$

f) $p = +1$:

$$A = (-\tfrac{1}{2})!,\ \sigma' = \tfrac{15}{4}\,\mathfrak{E}_{2.5}(x),\ \sigma'' = \tfrac{3}{2}\, x\mathfrak{E}_{1.5}(x).$$

The asymptotic form for $\mathfrak{E}_{2.5}$ was given in *b*). For $\mathfrak{E}_{1.5}$, when x is small

$$\mathfrak{E}_{1.5}(x) = \tfrac{1}{75}\,(1 - 0.667x^2 + 0.152x^4) - 2.363x^{1.5}\cos(0.785 + x);$$

when x is large

$$\mathfrak{E}_{1.5}(x) = y^2(1 - 8.75y^2).$$

g) $p = +1.5$:

$$A = 1,\ \sigma' = (3!)y^2\mathfrak{E}_3(y^2),\ \sigma'' = (1.5)!y\mathfrak{E}_{1.5}(y^2).$$

The asymptotic form of $\mathfrak{E}_3$ was given in *a*). For small values of y,

$$\mathfrak{E}_{1.5}(y^2) = -2.667y^2(1 + 0.761y^2) + 0.787y^{\frac{5}{3}}\exp(y^{\frac{2}{3}})\cos(1.047 - 0.865y^{\frac{2}{3}}).$$

For large values of y,

$$\mathfrak{E}_{1.5}(y^2) = 1 - 39.4x^2.$$

Appendix 2

To show that σ'' makes $\pm 90°$ intersections with the σ'-axis, we observe,

$$\frac{\partial\sigma''}{\partial\sigma'} = \frac{\partial}{\partial x}\int \frac{x\varepsilon^{\frac{1}{2}}e^{-\varepsilon}}{\varepsilon^{2p} + x^2}\,d\varepsilon \Big/ \frac{\partial}{\partial x}\int \frac{\varepsilon^{\frac{1}{2}+p}e^{-\varepsilon}}{\varepsilon^{2p} + x^2}\,d\varepsilon.$$

The numerator becomes

$$\left(1 + x\frac{\partial}{\partial x}\right)\int \frac{\varepsilon^{\frac{1}{2}}e^{-\varepsilon}}{\varepsilon^{2p} + x^2}\,d\varepsilon.$$

When $x \to 0$, the first term is finite, the second term and the denominator term approach zero from the negative value. Therefore,

$$\frac{\partial\sigma''}{\partial\sigma'} \to -\infty.$$

When $x \to \infty$, all integrals become power functions of x with power -2, and

$$\frac{\partial\sigma''}{\partial\sigma'} \to 0(x) + \infty.$$

Therefore, σ'' intersects the σ'-axis at $+90°$, when $\omega \to \infty$ and at $-90°$, when $\omega = 0$.

Received 30th July, 1960.

References

1) *a.* Phelps, A., V. Fundingsland and S. C. Brown, Phys. Rev. **84** (1951) 559.
   b. Allis, W. P., Handb. Phys., Springer-Verlag, Berlin 1956, Vol. 21, p. 413.
   c. Margenau, H., Phys. Rev. **69** (1946) 508; **109** (1958) 6.
   d. Molmud, P., Phys. Rev. **114** (1959) 29.
2) *a.* Wilson, A. H., The Theory of Metals, Cambridge University Press 1953, p. 196.
   b. Blatt, F. J., in Solid State Physics, Academic Press Inc., N.Y. 1955, Vol. 4, p. 199-366.
   c. Bronstein, M., Physik. Z. Sowjetunion **2** (1932) 28.
   d. Conwell, E. M., and V. Weisskopf, Phys. Rev. **77** (1950) 388.
   e. Stolz, H., Ann. Phys. Lpz. **19** (1957) 394; **1** (1958) 334.
3) Cohen, L., Spitzer and Routly, Phys. Rev. **80** (1950) 230; L. Spitzer and R. Harm, *ibid.* **89** (1952) 977.
4) Massey, H. S. W. and E. H. S. Burhop, Electronic and Ionic Impact Phenomena, Clarendon Press, Oxford 1952, p. 208; S. Altshuler, Phys. Rev. **107** (1957) 114.
5) Gould, L. and S. C. Brown, Phys. Rev. **95** (1957) 897.

6) Crompton, Huxley and Sutton, Proc. Roy, Soc. (London) A **218** (1953) 507.
7) Phelps, A. V. and J. L. Pack, Phys. Rev. Letters **3** (1959) 340; J. Schneider and F. W. Hoffman, Phys. Rev. **116** (1959) 244.
8) Koshino, S., Prog. Theoret. Phys. Japan **18** (1957) 23.
9) Howarth, D. J. and E. A. Sondheimer, Proc. Roy. Soc. (London) A **219** (1953) 53; H. Stolz, Ann. Phys. Lpz **19** (1957) 394; **1** (1958) 334.
10) Fang, P. H., Phys. Rev. **113** (1959) 13; P. H. Fang Ann. Phys. Lpz **7** (1960) 113.
11) Dingle, R. B., D. Arndt and S. K. Roy, Appl. Sci. Res. B **6** (1957) 144, 155, 245.
12) Cole, K. S. and R. H. Cole, J. Chem. Phys. **19** (1941) 1484.
13) Sodha, M. S. and Y. P. Varshni, Phys. Rev. **114** (1959) 717.
14) See, for example, J. Ross Macdonald and Malcolm K. Brachman, Rev. Mod. Phys. **28** (1956) 393.
15) This is pointed out to me by Dr. A. D. Franklin.
16) This distribution function is consistent with the formulation used in ref. [2b]), p. 240.
17) Fang, P. H., Physica **24** (1958) 970; P. H. Fang and M. Newman (to be submitted to J. Chem. Phys.).
18) This average is also involved in the deviation of the conductivity of semiconductors in a weak magnetic field. See H. Brooks, Advances in Electronics and Electron Physics, Academic Press. N.Y. 1955, Vol. 7, p. 128. See also ref. [16]).
19) A problem of somewhat similar nature occurs in the calculation of mobility due to Ramsauer scattering. The mobility becomes infinite (Yu. U. Gulyaev, Soviet J. Solid State Phys. **1** (1959) 422, Transl. Soviet Phys., Solid State Phys. **1** (1959) 381. A simple mathematical example where the distribution function is well behaved but no expectancy is definable was discussed by J. V. Uspensky, Introduction to Mathematical Probability, McGraw-Hill Book Co. 1937, p. 242.
20) Sodha, M. S. and Y. P. Varshni, Phys. Rev. **114** (1959) 946.

Appl. sci. Res. Section B, Vol. 9

ELECTROMAGNETIC GENERATION OF VORTICITY IN THE UNIFORM EFFLUX OF A CONDUCTING FLUID FROM THE SURFACE OF A MAGNETIZED SPHERE

by J. D. MURRAY

Mathematics Department, University College London, England

Summary

The electromagnetic forces in the flow of an electrically conducting fluid in the presence of a magnetic field are non-conservative and therefore produce vorticity. The simple case of uniform efflux of a conducting fluid from the surface of a magnetized sphere is studied. Two methods are developed: one gives the solution for small conductivity and any magnetic intensity, the other gives the solution for small magnetic intensity and any conductivity. The case evaluated in detail is that for a magnetic dipole situated at the centre of the sphere. The magnetic lines, streamlines and vortex lines are found in closed form and shown in figs. 1 and 2 for two values of the parameters involved.

§ 1. *Introduction.* In magnetohydrodynamics, the electromagnetic force is non-conservative and therefore produces vorticity. In all such flows of a conducting fluid the generation of this vorticity is of special interest.

In [1]), Ludford and Murray investigated the flow of an inviscid, incompressible, conducting fluid past a magnetized sphere: first order effects of the magnetic field and conductivity were studied. Due to the complexity of the solution for the vorticity, its behaviour was studied in detail only on the sphere, where it was found to be logarithmically infinite. The magnetic distribution was an axially symmetric one. In [2]), Murray and Chi showed that in the two dimensional case the appearence of such a singularity in the vorticity was critically dependent on the magnetic configuration in the body.

In [1]) and [2]), where the magnetic field originated in the body, it was shown that non-singular perturbations could not be made for

small R_M, the magnetic Reynolds number. The non-uniformity at infinity could be incorporated in an exponential factor similar to that found in Oseen's approximation in the viscous flow past a sphere. In the magnetohydrodynamic viscous flow past a semi-infinite flat plate Greenspan and Carrier [3]) and Murray [4]) show that an expansion in R_M is not possible when the magnetic field is externally applied in the direction of fluid flow at infinity.

The investigation below is concerned with the steady efflux of an incompressible inviscid conducting fluid from the surface of a sphere in which a magnetic field originates. The methods are developed for a general magnetic distribution. In this situation, for zero conductivity, the fluid velocity and magnetic intensity tend to zero algebraically at large distances from the sphere. The simplest case in which the electromagnetic body force is non-zero is that in which the fluid field (for zero R_M) is represented mathematically by a source at the centre of the sphere, which is considered to be uniformly magnetized, i.e. a magnetic dipole is situated at the centre. Here the undisturbed fluid velocity vector is not parallel to the magnetic intensity vector and vorticity will thus be created. For such a configuration the current lines and vortex lines are circles.

In the case discussed in § 3 below, it is shown that a simple perturbation in the magnetic Reynolds number R_M *is* uniformly valid for all values of β, the ratio of a representative magnetic pressure to a representative fluid dynamic pressure. On the other hand, for small values of β, a simple perturbation can be found in β for all R_M (see § 4). If the latter solution to first order in β is then expanded for small R_M, it agrees with the former. Closed form solutions can be found to any order of R_M or β for the magnetic field, the electric current, the fluid velocity and the vorticity. The case worked out in detail is that for small R_M: no difficulties are encountered for large R_M. The streamlines, constant magnetic field lines and vortex lines are shown in figs. 1 and 2 for various values of the parameters involved.

The flow is completely independent of the conductivity of the sphere as long as it is finite. If the magnetic field is originally assumed to be frozen into the sphere (i.e. the sphere has infinite conductivity), the results are different: these are given in § 5.

Astronomically it is of interest to consider pressure balanced

magnetic fields in the atmosphere of the sun (see e.g. [5]), which may be considered to be a uniformly magnetized sphere. In this, the efflux of an infinitely conducting gas from the surface distorts the magnetic lines and pushes them outwards from the centre like elastic strings under tension, until the magnetic pressure balances the fluid pressure. If the conductivity of the gas is finite, the field lines are still pushed out, but the steady state then consists of the fluid passing across the field lines in their displaced position. This is similar to the problem discussed below. Accordingly, the case worked out in detail is that for a dipole situated at the centre of the sphere. With the method described below, the fluid pressure distribution on the surface of the sphere can be varied easily by addition of further fluid sources and sinks inside the sphere as long as axial symmetry is preserved.

§ 2. *Basic equations and their non-dimensional form.* Neglecting the displacement current, the equations governing the steady flow of an electrically conducting, incompressible, inviscid fluid of constant properties are

$$\operatorname{div} \boldsymbol{q} = 0, \tag{1}$$

$$\operatorname{curl} \boldsymbol{q} \times \boldsymbol{q} = -\operatorname{grad} (p/\rho + \tfrac{1}{2}\boldsymbol{q}^2) + \frac{\mu}{\rho} \boldsymbol{j} \times \boldsymbol{H}, \tag{2}$$

$$\boldsymbol{j} = \operatorname{curl} \boldsymbol{H} = \sigma(\boldsymbol{E} + \mu \boldsymbol{q} \times \boldsymbol{H}), \tag{3}$$

$$\operatorname{div} \boldsymbol{H} = 0 = \operatorname{curl} \boldsymbol{E}, \tag{4}$$

where μ and σ are the magnetic permeability and conductivity of the fluid respectively, and $\boldsymbol{q}$, p, ρ, $\boldsymbol{j}$, $\boldsymbol{H}$ and $\boldsymbol{E}$ have the usual meanings.

The specific three-dimensional geometry considered is that of a sphere of radius a, situated at the origin $r = 0$, where r and θ are the axially symmetric polar coordinates as in fig. 1. The uniform efflux of fluid is simulated mathematically by a source at the origin. The magnetic field $\boldsymbol{H}$, which originates in the sphere, and the velocity $\boldsymbol{q}$ lie in the meridian plane and are independent of the azimuthal angle (see figs. 1 and 2). From the conduction equation (3) the electric field $\boldsymbol{E}$ is perpendicular to the meridian plane, and from the second of (4), $\boldsymbol{E} = 0$ if it is to be finite on the axis.

The quantities $\boldsymbol{q}$, $\boldsymbol{H}$ and r are made dimensionless by referring them to the velocity U at the surface of the sphere, a representative

magnetic intensity h, and the radius of the sphere a, respectively. The equations in non-dimensional form become (retaining the same symbols for their non-dimensional form)

$$\operatorname{div} \boldsymbol{q} = 0, \tag{5}$$

$$\operatorname{curl} \boldsymbol{q} \times \boldsymbol{q} = -\operatorname{grad} P + \beta \operatorname{curl} \boldsymbol{H} \times \boldsymbol{H}, \tag{6}$$

$$\operatorname{curl} \boldsymbol{H} = R_M \boldsymbol{q} \times \boldsymbol{H}, \tag{7}$$

$$\operatorname{div} \boldsymbol{H} = 0, \tag{8}$$

where $P = p + \frac{1}{2}\boldsymbol{q}^2$, $\beta = \mu h^2/\rho U^2$, $R_M = Ua\mu\sigma$ and p is now the pressure divided by ρU^2.

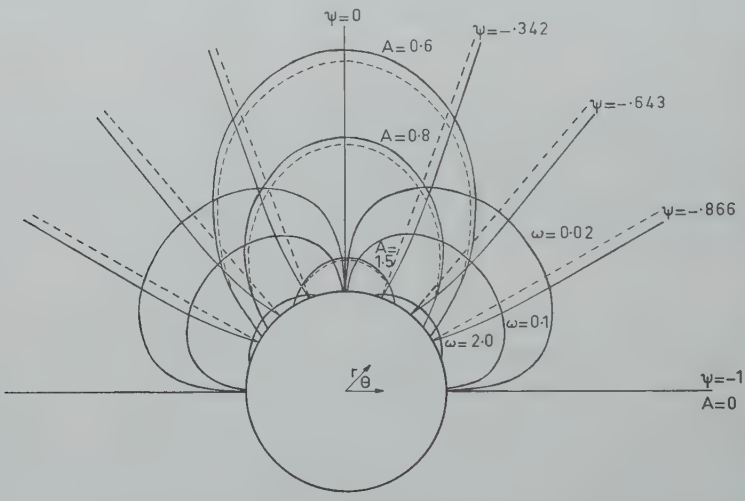

Fig. 1. Magnetic and fluid field lines when $R_m = 0.2$, $\beta = 5$, $\mu' = 2\mu$ and σ' is finite.

When $R_M = 0$, or $\beta = 0$, the streamlines are straight lines and the velocity is given by

$$\boldsymbol{q} = \boldsymbol{q}_0 = (1/r^2,\ 0,\ 0). \tag{9}$$

In the axially symmetric case, $\boldsymbol{H} = (H_r,\ H_\theta,\ 0)$ and

$$H_r = \frac{1}{r^2 \sin\theta} \frac{\partial A}{\partial \theta}, \quad H_\theta = -\frac{1}{r \sin\theta} \frac{\partial A}{\partial r}, \tag{10}$$

where A is a function of r and θ alone.

§ 3. *The perturbation in* R_M. For small conductivity we expand in powers of R_M and write

$$\boldsymbol{q} = \boldsymbol{q}_0 + R_M \boldsymbol{q}_1 + \ldots, \qquad \boldsymbol{H} = \boldsymbol{H}_0 + R_M \boldsymbol{H}_1 + \ldots,$$
$$p = p_0 + R_M p_1 + \ldots \qquad (11)$$

Substitution of (11) in (5) to (8) gives $\boldsymbol{q}_0$ as in (9) and the non-zero component of (7) as

$$\frac{\partial^2 A_0}{\partial r^2} + \frac{\sin\theta}{r^2}\frac{\partial}{\partial\theta}\left(\frac{1}{\sin\theta}\frac{\partial A_0}{\partial\theta}\right) = 0, \qquad (12)$$

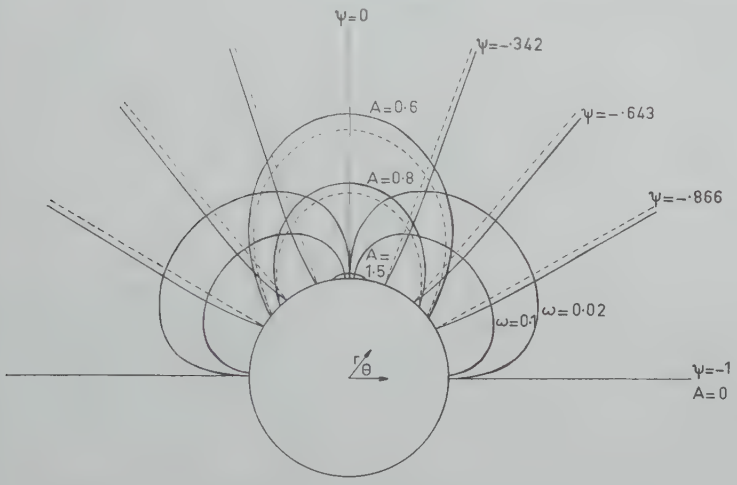

Fig. 2. Magnetic and fluid field lines when $R_m = 0.2$, $\beta = 5$, $\mu' = 2\mu$ and σ' is infinite.

Inside the sphere $\boldsymbol{E} = 0$ again, and so curl $\boldsymbol{H} = \sigma'\boldsymbol{E} = 0$, where σ' is the conductivity of the sphere. Thus, inside the sphere A_0 (and also A_i, $i \geqslant 1$) satisfies (12).

Any axially symmetric distribution which is a solution of (12) can be taken. In the specific case here considered, i.e. that of a dipole situated at the origin pointing in the direction $\theta = 0$ (figs. 1 and 2), the potential A_0 which satisfies the boundary conditions on the sphere (continuity of the normal component of magnetic induction and tangential component of magnetic field) and tends to zero at infinity is

$$A_0(r,\theta) = \frac{3\mu'}{2\mu+\mu'}\frac{\sin^2\theta}{r}, \quad \text{for } r \geqslant 1,$$
$$A_0(r,\theta) = \frac{\sin^2\theta}{r} + \frac{\mu-\mu'}{2\mu+\mu'} r^2 \sin^2\theta, \text{ for } r \leqslant 1, \qquad (13)$$

where μ' is the magnetic permeability of the sphere.

The equations for $\boldsymbol{q}_1$ and $\boldsymbol{H}_1$ are

$$\operatorname{div} \boldsymbol{q}_1 = \operatorname{div} \boldsymbol{H}_1 = 0, \tag{14}$$

$$\operatorname{curl} \boldsymbol{q}_1 \times \boldsymbol{q}_0 = -\operatorname{grad} P_1 + \beta \operatorname{curl} \boldsymbol{H}_1 \times \boldsymbol{H}_0, \tag{15}$$

$$\operatorname{curl} \boldsymbol{H}_1 = \boldsymbol{q}_0 \times \boldsymbol{H}_0, \tag{16}$$

$\boldsymbol{H}_1$ and $\boldsymbol{q}_1$ are found simultaneously. The non-zero component of (16) gives the equation for the potential A_1 (of $\boldsymbol{H}_1$) as

$$\frac{\partial^2 A_1}{\partial r^2} + \frac{\sin\theta}{r^2}\frac{\partial}{\partial\theta}\left(\frac{1}{\sin\theta}\frac{\partial A_1}{\partial\theta}\right) = -\left(\frac{3\mu'}{2\mu+\mu'}\right)\frac{\sin^2\theta}{r^4}, \tag{17}$$

a particular integral of which is

$$-\frac{3}{4}\left(\frac{\mu'}{2\mu+\mu'}\right)\frac{\sin^2\theta}{r^2}.$$

To this solution must be added the appropriate complementary functions of (17), (i.e. $\sin^2\theta P'_n(\cos\theta)\, r^n$, n an integer and $P_n(\cos\theta)$ the Legendre polynomial), so that the boundary conditions on the sphere are satisfied to $0(R_M)$. Inside the sphere, irrotational disturbances must be added to A_0 of $0(R_M)$ of the form

$$R_M r^n \sin^2\theta P'_n(\cos\theta),$$

which are solutions of (12). A little manipulation shows that the appropriate solutions satisfying the boundary conditions are

$$\begin{aligned} A_1 &= \frac{3}{4}\left(\frac{\mu'}{2\mu+\mu'}\right)\frac{\sin^2\theta}{r}\left[\frac{2(\mu+\mu')}{(2\mu+\mu')} - \frac{1}{r}\right], \quad \text{for } r \geqslant 1 \\ A_1 &= \frac{3}{2}\frac{\mu\mu'}{(2\mu+\mu')^2} r^2 \sin^2\theta, \quad \text{for } r \leqslant 1. \end{aligned} \tag{18}$$

With A_0 and A_1 from (13) and (18), $A = A_0 + R_M A_1$ satisfies the equations and boundary conditions to $0(R_M)$ and from (10) the components of magnetic field are given by

$$\begin{aligned} H_r &= \left(\frac{3\mu'}{2\mu+\mu'}\right)\frac{2\cos\theta}{r^3}\left\{1 + \frac{R_M}{4}\left[\frac{2(\mu+\mu')}{(2\mu+\mu')} - \frac{1}{r}\right]\right\}, \\ H_\theta &= \left(\frac{3\mu'}{2\mu+\mu'}\right)\frac{\sin\theta}{r^3}\left\{1 + \frac{R_M}{2}\left[\frac{(\mu+\mu')}{(2\mu+\mu')} - \frac{1}{r}\right]\right\}, \end{aligned} \tag{19}$$

outside the sphere, and

$$H_r = \frac{2\cos\theta}{r^3} + \left(\frac{\mu - \mu'}{2\mu + \mu'}\right) 2\cos\theta + R_M 3 \frac{\mu\mu'}{(2\mu + \mu')^2} \cos\theta,$$
$$H_\theta = \frac{\sin\theta}{r^3} - \left(\frac{\mu - \mu'}{2\mu + \mu'}\right) 2\sin\theta - R_M 3 \frac{\mu\mu'}{(2\mu + \mu')^2} \sin\theta, \tag{20}$$

inside the sphere: (18), (19), and (20) are correct to $0(R_M)$,

The vorticity vector, curl $\boldsymbol{q}_1$, is perpendicular to the meridian plane and has therefore only one component ω_1. From (15)

$$0 = -\frac{\partial P_1}{\partial r} + \beta F_r,$$
$$\frac{\omega_1}{r^2} = -\frac{1}{r}\frac{\partial P_1}{\partial \theta} + \beta F_\theta, \tag{21}$$

where $\boldsymbol{F} = (F_r, F_\theta, 0) = \operatorname{curl} \boldsymbol{H}_1 \times \boldsymbol{H}_0 = (\boldsymbol{q}_0 \times \boldsymbol{H}_0) \times \boldsymbol{H}_0$, so

$$F_r = -\left(\frac{3\mu'}{2\mu + \mu'}\right)^2 \frac{\sin^2\theta}{r^8}, \quad F_\theta = \left(\frac{3\mu'}{2\mu + \mu'}\right)^2 \frac{\sin 2\theta}{r^8}.$$

From (21), since ω_1 is finite at infinity,

$$\omega_1 = \beta\frac{6}{7}\left(\frac{3\mu'}{2\mu + \mu'}\right)^2 \frac{\sin 2\theta}{r^6}, \quad P_1 = \beta\frac{1}{7}\left(\frac{3\mu'}{2\mu + \mu'}\right)^2 \frac{\sin^2\theta}{r^7}, \tag{22}$$

Thus, $\boldsymbol{\omega} = (0, 0, \omega) = (0, 0, R_M\omega_1)$ to $0(R_M)$, with ω_1 given by (22) for *all* β. Lines of constant vorticity are shown in figs. 1 and 2.

The velocity vector is easily found from $\boldsymbol{q}_0$ and ψ_1, where ψ_1 is the Stokes stream function for $\boldsymbol{q}_1$ and

$$\frac{\partial^2\psi_1}{\partial r^2} + \frac{\sin\theta}{r^2}\frac{\partial}{\partial\theta}\left(\frac{1}{\sin\theta}\frac{\partial\psi_1}{\partial\theta}\right) = -r\sin\theta\omega_1, \tag{23}$$

with ω_1 from the first of (22). The boundary conditions on ψ_1 are $\psi_1 \to 0$ as $r \to \infty$, and the normal component on the sphere is zero. The appropriate solution of (23) is

$$\psi_1 = \beta\frac{2}{7}\left(\frac{3\mu'}{2\mu + \mu'}\right)^2 \frac{\sin^2\theta\cos\theta}{r^2}\left(1 - \frac{1}{r}\right), \tag{24}$$

and

$$\boldsymbol{q}_1 = (q_{1r}, q_{1\theta}, 0)$$
$$= \beta\frac{2}{7}\left(\frac{3\mu'}{2\mu+\mu'}\right)^2\left[\frac{(3\cos^2\theta - 1)}{r^4}\left(1 - \frac{1}{r}\right), \frac{\sin 2\theta}{2r^4}\left(2 - \frac{3}{r}\right), 0\right]. \tag{25}$$

The streamlines are given by $\psi = \psi_0 + R_M\psi_1 =$ constant, where $\psi_0 = -\cos\theta$, giving $\boldsymbol{q}_0 = (1/r^2, 0, 0)$ and are shown in figs. 1 and 2 for two values of σ', and given R_M and β. Note that (24) and (25) hold for *all* β.

Higher order terms in R_M can be easily found, also, for *all* β.

Note that the ratio of any term to the preceding one in the $\boldsymbol{q}$ series tends to zero as $r \to \infty$, whereas the similar ratio in the $\boldsymbol{H}$ series tends to a term of $0(R_M)$. This is not, however, surprising since in the interaction of $\boldsymbol{H}_0$ and $\boldsymbol{q}_0$, $\boldsymbol{H}_0 = 0\,(1/r^3)$, and $\boldsymbol{q}_0 = 0(1/r^2)$ for large r.

§ 4. *The perturbation in* β. In the above section, closed form expressions were obtained for $\boldsymbol{H}$, $\boldsymbol{q}$ and $\boldsymbol{\omega}$ for all β and small R_M. If, on the other hand, solutions are sought for *all* R_M, a simple expansion for β can be taken, similar to that in [1]) and [2]). Here we write

$$\boldsymbol{q} = \boldsymbol{q}_0 + \beta\boldsymbol{q}_1 + \ldots, \quad \boldsymbol{H} = \boldsymbol{H}_0 + \beta\boldsymbol{H}_1 + \ldots, \quad p = p_0 + \beta p_1 + \ldots \tag{26}$$

Here, $\boldsymbol{H}_0$ is not the undisturbed field since, to get the dimensional magnetic field, $\boldsymbol{H}_0$ must be multiplied by h, which is proportional to $\beta^{\frac{1}{2}}$, and it is this quantity which would tend to zero as $\beta \to 0$.

On substitut ng (26) in (5) and (6), $\boldsymbol{q}_0$ is again given by (9), and (7) and (8) become

$$\operatorname{curl} \boldsymbol{H}_0 = R_M \boldsymbol{q}_0 \times \boldsymbol{H}_0, \quad \operatorname{div} \boldsymbol{H}_0 = 0. \tag{27}$$

Using (10), the non-zero component of the first of (27) is

$$\frac{\partial^2 A_0}{\partial r^2} + \frac{\sin\theta}{r^2}\frac{\partial}{\partial\theta}\left(\frac{1}{\sin\theta}\frac{\partial A_0}{\partial\theta}\right) = R_M \frac{1}{r^2}\frac{\partial A_0}{\partial r}, \tag{28}$$

simple product solutions of which are

$$A_0(r, \theta; R_M) = F_n(r/R_M)\sin^2\theta\, P'_n(\cos\theta), \tag{29}$$

where n is a positive integer, P'_n the derivative of the Legendre polynomial, and

$$F_n(r/R_M) = (R_M/r)^n f_n(R_M/r)\exp(-R_M/r), \tag{30}$$

with

$$f_n(R_M/r) = 1 + \frac{(n+2)}{1!(2n+2)}\frac{R_M}{r} + \frac{(n+2)(n+3)}{2!(2n+2)(2n+3)}\left(\frac{R_M}{r}\right)^2 + \ldots \tag{30}$$

(see Whittaker and Watson [6]), Chapter XVI,). For fixed r,

$$R_M^{-n} A_0 \to \sin^2\theta P'_n(\cos\theta)/r^n \quad \text{as} \quad R_M \to 0;$$

i.e. solutions of curl $\boldsymbol{H}_0 = 0$, as it must.

The solution of (28) is now found by adding to the appropriate solution (29) complementary functions of (28) so that the boundary conditions on the sphere are satisfied for *all* R_M. For a dipole situated at the origin, the appropriate solution to take is

$$A_0 = K \frac{\sin^2\theta}{r} f_1(R_M/r) \exp(-R_M/r), \qquad (r \geqslant 1), \tag{31}$$

the solution $n = 1$, where K must be determined from the boundary conditions on the sphere. From (30),

$$f_1(R_M/r) = 1 + \frac{3}{4}\frac{R_M}{r} + \frac{3}{2\,!\,5}\left(\frac{R_M}{r}\right)^2 + \frac{3}{3\,!\,6}\left(\frac{R_M}{r}\right)^3 + \ldots$$

The potential inside the sphere is of the form

$$A_0 = \frac{\sin^2\theta}{r} + kr^2 \sin^2\theta, \qquad (r \leqslant 1), \tag{32}$$

where k is determined in conjunction with K. The representative field h can now be identified as $M\,a^3$, where M is the moment of the dipole. Using (31) and (32), the continuity of the normal component of magnetic induction and the tangential component of magnetic field give

$$\begin{aligned} K &= \frac{3\mu' \exp(R_M)}{2\mu f_1(R_M) + \mu'\{f_1(R_M) - R_M[f_1(R_M) - f_1'(R_M)]\}}, \\ k &= \frac{(\mu - \mu')\, f_1(R_M) + R_M\mu'\,[f_1(R_M) - f_1'(R_M)]}{2\mu f_1(R_M) + \mu'\{f_1(R_M) - R_M[f_1(R_M) - f_1'(R_M)]\}}, \end{aligned} \tag{33}$$

where the dash on f_1 denotes differentiation with respect to the argument. The components of the magnetic field are given by

$$\begin{aligned} H_{0r} &= K\frac{2\cos\theta}{r^3} f_1(R_M/r) \exp(-R_M/r), \\ H_{0\theta} &= K\frac{\sin\theta}{r^3}\left\{f_1(R_M/r) - \frac{R_M}{r}[f_1(R_M/r) - f_1'(R_M/r)]\right\}\exp(-R_M/r), \end{aligned} \tag{34}$$

outside the sphere, and by

$$H_{0_r} = \frac{2\cos\theta}{r^3} + 2k\cos\theta, \qquad H_{0_\theta} = \frac{\sin\theta}{r^3} - 2k\sin\theta, \tag{35}$$

inside the sphere, with K and k from (33).

When R_M is small,

$$f_1(R_M/r)\exp(-R_M/r) = 1 - R_M/r + 0(R_M{}^2/r^2),$$

$$K = \left(\frac{3\mu'}{2\mu+\mu'}\right)\left[1 + R_M\frac{(\mu+\mu')}{2(2\mu+\mu')}\right] + 0(R_M{}^2),$$

$$k = \left(\frac{\mu-\mu'}{2\mu+\mu'}\right)\left[1 + \frac{3R_M\mu\mu'}{4(2\mu+\mu')(\mu-\mu')}\right] + 0(R_M{}^2),$$

and (31) and (32) give the same result as the sum of (13) and (18) to the same order in R_M. The vorticity ω_1, the stream function ψ_1 and the velocity $\boldsymbol{q}_1$ are then given by (22) (24) (25) respectively to $0(R_M)$, and the magnetic, fluid and vortex lines are as in figs. 1 and 2, even though β is not small.

For *all* R_M, the vorticity $\boldsymbol{\omega}_1 = (0, 0, \omega_1)$, from (26) and (6), is the solution of

$$\boldsymbol{\omega}_1 \times \boldsymbol{q}_0 = -\operatorname{grad} P_1 + R_M(\boldsymbol{q}_0 \times \boldsymbol{H}_0) \times \boldsymbol{H}_0,$$

where $\boldsymbol{H}_0$ is now obtained from (31). The non-zero components of the last equation give

$$0 = \frac{\partial P_1}{\partial r} + \frac{R_M}{r^2}(H_{0_\theta})^2, \qquad \frac{\omega_1}{r} = -\frac{\partial P_1}{\partial\theta} + \frac{R_M}{r}(H_{0_\theta}H_{0_r}),$$

with H_{0_r}, H_{0_θ} from (34). The non-zero component of the vorticity $\boldsymbol{\omega}$ is, to $0(\beta)$,

$$\omega = \beta\omega_1 = K^2\beta R_M\sin 2\theta\left\{\frac{\exp(-2R_M/r)}{r^6}f_1(R_M/r)\cdot\right.$$

$$\left.\cdot\,[f_1(R_M/r) - (R_M/r)\{f_1(R_M/r) - f_1'(R_M/r)\}] + \right.$$

$$\left. + r\int_\infty^r \frac{\exp(-2R_M/r)}{r^8}[f_1(R_M/r) - (R_M/r)\{f_1(R_M/r) - f_1'(R_M/r)\}]^2 \mathrm{d}r\right\}, \tag{36}$$

where the lower limit, infinity, in the integral ensures finiteness of ω as $r \to \infty$. For small R_M, (36) gives (22) to $0(R_M)$. For large R_M the $f_1(R_M\, r)$ series in (30) is used: the series converges quite rapidly. Equation (36) can be integrated term by term with $f_1(R_M\, r)$ taken up to the last term used in the summation to obtain A_0. The stream function and velocity can be found in the same way as in § 3 to any degree of accuracy required for any finite R_M.

§ 5. *The perfectly conducting sphere.* The above analysis is for a sphere of arbitrary conductivity σ', however large, as long as it remains finite. The final expressions for the magnetic and fluid field do not involve σ'. For the case of infinite conductivity, the magnetic field is frozen into the sphere and the boundary conditions on the magnetic field are different as are the results.

For the dipole case above, the field inside the sphere is always given by $\boldsymbol{H} = \operatorname{curl}(0, 0, r^{-1} \sin^2\theta)$. The only condition on the field outside the sphere is now that of continuity of the normal component of magnetic induction: there is no condition on the tangential component of magnetic field. The first equation of (18), the first of (22) and (24) become respectively

$$\begin{aligned} A_1 &= \frac{1}{4}\left(\frac{\mu'}{\mu}\right)\frac{\sin^2\theta}{r}\left(1 - \frac{1}{r}\right), \\ \omega_1 &= \beta\frac{6}{7}\left(\frac{\mu'}{\mu}\right)^2\frac{\sin 2\theta}{r^6}, \\ \psi_1 &= \beta\frac{2}{7}\left(\frac{\mu'}{\mu}\right)^2\frac{\sin^2\theta\cos\theta}{r^2}\left(1 - \frac{1}{r}\right), \end{aligned} \tag{37}$$

and (31) becomes

$$A_0 = \left(\frac{\mu'}{\mu}\right)\frac{\sin^2\theta}{r}\,\frac{f_1(R_M r)}{f_1(R_M)}\exp[R_M(1 - 1/r)], \tag{38}$$

while the vorticity is the same as (36) with K^2 replaced by

$$\left(\frac{\mu'}{\mu}\right)^2\frac{\exp(2R_M)}{[f_1(R_M)]^2}.$$

Thus, the assumption of infinite conductivity in the sphere would

lead to an error, in the magnetic field say, in § 4 by a factor

$$\frac{K}{(\mu'/\mu)\, f_1(R_M) \exp R_M} =$$

$$= \frac{3\mu}{f_1(R_M)[2\mu f_1(R_M) + \mu'\{f_1(R_M) - R_M[f_1(R_M) - f_1'(R_M)]\}]},$$

and comparable factors in the fluid field.

Figs. 1 and 2 illustrate the difference in the magnetic field and fluid field for $R_M = 0.2$, $\beta = 5$, $\mu' = 2\mu$, and σ' finite and infinite respectively.

Received 20th August, 1960.

REFERENCES

1) Ludford, G. S. S. and J. D. Murray, J. Fluid Mechanics **7** (1960) 516.
2) Murray, J. D. and L. Chi, Mathematika **7** (1960) 64.
3) Greenspan, H. P. and G. F. Carrier, J. Fluid Mechanics **6** (1959) 77.
4) Murray, J. D., Magnetohydrodynamic Flow past a flat Plate in the Presence of an adverse Pressure Gradient (in preparation).
5) Lundqvist, S., Ark. Fys. **2** (1950–51) 361.
6) Whittaker, E. T. and G. N. Watson, Modern Analysis, Cambridge University Press, Cambridge 1949.

ISENTROPIC ONE-DIMENSIONAL MAGNETOHYDRODYNAMIC CHANNEL FLOW

by BORIS PODOLSKY

University of Cincinnati, Cincinnati, Ohio, U.S.A.

and A. SHERMAN

General Electric Company, Cincinnati, Ohio, U.S.A.

Summary

It is usual in the analysis of one-dimensional channel flows to study the behaviour of the analogous isentropic flow since, first, it retains the essential features of flows of practical interest and, secondly, it is simpler to describe. Although in conventional channel flows it is sufficient to neglect heat addition and friction to ensure isentropicity, in the MHD case it is in addition necessary to neglect Joule heating. This is accomplished by considering the fluid as having infinite electrical conductivity. However, this procedure does not necessarily imply infinite currents, since the external resistance will limit current flow. In the conventional problem, if we assume an isentropic flow, we are able to obtain a once integrated form of the governing equations. Such once integrated solutions are not possible in the present isentropic MHD channel flow, but equally simple solutions can be found and are presented. Examples of application of these results to the crossed field MHD generator and accelerator are also given.

§ 1. *Introduction.* Application of the crossed field generator to the large scale generation of electrical power [1]) and of the crossed field accelerator to space propulsion [2]) has stimulated considerable interest in MHD channel flows in general. The purpose of this paper is to propose a simple procedure for studying their behaviour.

As is well known, a useful approximation for the analysis of channel flows is to assume that the flow is quasi-one dimensional. Such an approach permits a considerable simplification and will be followed in the present study. We also know that the analysis of the resulting one-dimensional equations will be complicated by the presence of the Lorentz force and Joule heating terms [3]). Therefore, a further simplification would be to neglect Joule heating.

If we also neglect heat conduction and viscous dissipation, and if we require that changes of state occur very slowly, the flow may be considered isentropic.

However, the Joule heating can only be neglected if the fluid conductivity is assumed to be infinite. Normally, in the study of unconfined flows this assumption implies no relative motion between the fluid and the magnetic lines of force, since any such motion would induce infinite currents. In the present confined channel flow, though, such relative motion is possible, since the current flow is limited by the external resistance. Therefore, in the following analysis we will make such an assumption and study the resulting, simplified equations.

§ 2. *Analysis.* The basic equations for the steady flow of a perfect, non-viscous, non-heat conducting gas of infinite electrical conductivity can be written as follows:
momentum:

$$\rho(\boldsymbol{v}\cdot\nabla)\,\boldsymbol{v} + \nabla p = \boldsymbol{i} \times \boldsymbol{B}, \tag{1}$$

isentropicity:

$$\nabla(p/\rho^{\gamma}) = 0, \tag{2}$$

continuity:

$$\nabla\cdot(\rho\boldsymbol{v}) = 0, \tag{3}$$

Ohm's law:

$$\boldsymbol{E} + \boldsymbol{v} \times \boldsymbol{B} = 0, \tag{4}$$

Maxwell's equation:

$$\boldsymbol{i} = \frac{1}{\mu_e}\nabla \times \boldsymbol{B}, \tag{5}$$

where we have used the rationalized MKS system of units and where $\boldsymbol{v}$ is the gas velocity vector, p the gas pressure, ρ the mass density, γ the isentropic constant, $\boldsymbol{i}$ the current density vector, $\boldsymbol{E}$ the electric field intensity vector, $\boldsymbol{B}$ the magnetic induction vector and μ_e the magnetic permeability, which is assumed constant. If we recall that the total magnetic field can be considered as the sum of an applied and an induced field and observe that within the channel the applied field must be irrotational, then (5) can be written as

$$\boldsymbol{i} = \frac{1}{\mu_e}\nabla \times \boldsymbol{b}, \tag{6}$$

where $\boldsymbol{b}$ is the induced magnetic induction vector.

Next we consider the flow through a channel of slowly varying cross-sectional area, such as that shown in fig. 1. For this geometry we employ the usual assumptions of quasi-one-dimensional flow. That is, we consider that there is only an x-component of velocity u, a z-component of applied magnetic field B, y-components of electric field E and current density i, and that these along with the pressure and density are functions only of x. The z-component of induced magnetic field has been shown by McCune and Sears [4]) to be negligible for infinitely long channels of slowly varying height and, therefore, will be neglected. They have also pointed out that the x-component of induced magnetic field within the channel varies linearly with and is an odd function of z, so that its average value is zero. Since our one-dimensional approach considers only average quantities, this is consistent with our assumption of a pressure p which is a function of x alone.

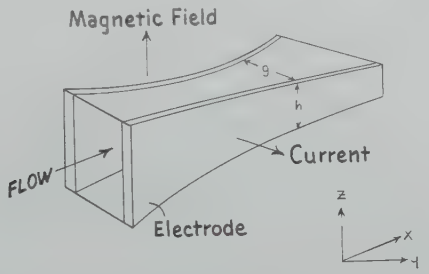

Fig. 1. Configuration of general MHD channel with crossed electric and magnetic fields.

If we then neglect both components of the induced magnetic field, we obtain the following simplified set of equations.

$$\rho u \frac{\mathrm{d}u}{\mathrm{d}x} + \frac{\mathrm{d}p}{\mathrm{d}x} = iB, \tag{7}$$

$$\frac{\mathrm{d}}{\mathrm{d}x}\left(p/\rho^{\gamma}\right) = 0, \tag{8}$$

$$\frac{\mathrm{d}}{\mathrm{d}x}\left(\rho u A\right) = 0, \tag{9}$$

$$E = UB, \tag{10}$$

where A is the channel cross-sectional area, which can be a function of x, and (9) is the continuity equation appropriate for the study of one-dimensional channel flow.

Before entering into a discussion of particular solutions to these equations, some general observations would be of value. The variable E can be omitted from consideration initially, since with B a given function of x, it can be found once u is obtained from the solution of (7), (8) and (9). There remain, therefore, three equations to be solved for the five variables u, p, ρ, A and i. Thus, in order to solve the problem, we must specify the x-dependence of two of these variables and give the initial values of the remaining three.

Equations (7), (8) and (9) can now be rewritten as follows:

$$\rho u \frac{\mathrm{d}u}{\mathrm{d}x} + \frac{\mathrm{d}p}{\mathrm{d}x} = iB, \tag{11}$$

$$\frac{p_0}{\rho_0{}^\gamma} = \frac{p}{\rho^\gamma}, \tag{12}$$

$$\rho_0 u_0 A_0 = \rho u A. \tag{13}$$

If the Lorentz force term iB in (11) were to be taken to be zero. then (11), (12) and (13) would describe a conventional isentropic flow. In this case, the equations can be integrated once and become

$$\frac{u_0{}^2}{2} + \frac{\gamma}{\gamma - 1}\frac{p_0}{\rho_0} = \frac{u^2}{2} + \frac{\gamma}{\gamma - 1}\frac{p}{\rho}, \tag{14}$$

$$\frac{p_0}{\rho_0{}^\gamma} = \frac{p}{\rho^\gamma}, \tag{15}$$

$$\rho_0 u_0 A_0 = \rho u A, \tag{16}$$

where the subscript zero denotes the value of the variable at some initial station. These equations can be handled in two different ways. First, we can specify the value of one of the variables at some downstream station and solve for the value of the other three variables at that station from the above equations. In this procedure, the distance between the initial and downstream stations is not specified, although it cannot be zero if all variables are to vary slowly with x. Another procedure would be to specify the x-variation of one of the four variables and solve for the other three as functions of x from

(14), (15) and (16). In this case, the distance between the initial station and one downstream is clearly defined, and although the calculation is not quite as easy, it is considerably more informative.

When the Lorentz force term is included to permit the study of isentropic one-dimensional MHD flows, a once integrated form of the equations, such as (14), (15) and (16), cannot be found. Solutions for the variables as functions of x can, however, be obtained by giving their initial values and specifying the x-variation of two of them. In the next section, two simple calculations will be made to illustrate this procedure.

§ 3. *Examples.* As a first example, let us consider a linearly increasing velocity and area so that we know

$$u = u_0 + ax; \quad A = A_0 + bx. \tag{17a,b}$$

In this case, (13) yields the variation of density with respect to x:

$$\rho = \frac{\rho_0 u_0 A_0}{abx^2 + (aA_0 + bu_0)\, x + u_0 A_0}. \tag{18}$$

Combining (12) and (18) gives an expression for the pressure which is

$$p = \frac{p_0 (u_0 A_0)^\gamma}{[abx^2 + (aA_0 + bu_0)\, x + u_0 A_0]^\gamma}. \tag{19}$$

To solve for i, we introduce $u(x)$ from (17a) along with $p(x)$ and $\rho(x)$ (equations (18) and (19)) into (11) and find the following result:

$$i = \frac{1}{B}\left\{\frac{\rho_0 u_0 A_0 (u_0 + ax)\, a}{abx^2 + (aA_0 + bu_0)\, x + u_0 A_0} - \right.$$
$$\left. - \frac{p_0 (u_0 A_0)^\gamma\, \gamma (2abx + aA_0 + bu_0)}{[abx^2 + (aA_0 + bu_0)\, x + u_0 A_0]^{\gamma+1}}\right\}, \tag{20}$$

where B is a function of x which remains to be specified. The channel geometry as well as the power consumed or generated can be determined with the aid of (10). We first define the electrode height as h and the spacing between electrodes as g, so that we can write

$$A = gh. \tag{21}$$

Then returning to (10), we substitute for $u(x)$ from (17a) to obtain

$$E = V/g = (u_0 + ax)\, B, \tag{22}$$

where V is the constant voltage between the electrodes. The electrode gap is, therefore, given by

$$g = \frac{V}{(u_0 + ax)\, B}. \tag{23}$$

The electrode height is thus available from (21) and (23):

$$h = \frac{(A_0 + bx)(u_0 + ax)\, B}{V}. \tag{24}$$

Finally, the total power generated or consumed is equal to the voltage V times the current flowing. The net current flowing for a channel of length L is simply the integral over x of the product of current density i and electrode height h. Therefore, the net power is calculated to be

$$P = \rho_0 u_0^2 A_0 aL + \rho_0 u_0 A_0 \frac{a^2 L^2}{2} -$$

$$- \frac{\gamma p_0 (u_0 A_0)^\gamma}{\gamma - 1} [(u_0 A_0)^{1-\gamma} - (abL^2 + (aA_0 + bu_0)\, L + u_0 A_0)^{1-\gamma}]. \tag{25}$$

This relation shows us that the net power is independent of the voltage V and applied magnetic field B and depends only on the initial conditions, the total channel length, and the assumed forms of u and A. The field B cannot, however, be made arbitrarily small since, according to (20), this would cause the current density to become extremely large. Such extreme current densities cannot be obtained in practice due to the fact that electron emission from electrode surfaces is limited. The constant voltage V primarily influences the values of g and h and, if not chosen properly, can make their ratio impractically large or small. In particular, it cannot be zero if $B \neq 0$, since then g would be zero and h infinite.

For our second example, we consider a case for which the current density i is given as a function of x. We then specify that the velocity u is constant, the applied magnetic field B is constant and and that the current density i increases linearly with x. We can then write

$$i = i_0 + cx,$$

and since u is constant, (11) reduces to

$$\frac{dp}{dx} = (i_0 + cx)\, B. \tag{26}$$

Integrating to obtain the pressure p we get

$$p = p_0 + Bx(i_0 + \tfrac{1}{2}cx). \tag{27}$$

The density is obtained from (12) and is given by

$$\rho = \frac{\rho_0}{p_0^{1/\gamma}} [p_0 + Bx(i_0 + \tfrac{1}{2}cx)]^{1/\gamma}, \tag{28}$$

and the area A is found by combining (28) and (13):

$$A = \frac{A_0 p_0^{1/\gamma}}{[p_0 + Bx(i_0 + \tfrac{1}{2}cx)]^{1/\gamma}}. \tag{29}$$

The power P can be calculated if we first obtain g from (10). Recalling that $E = V/g$, we have

$$g = V/u_0 B, \tag{30}$$

and the gap is constant for this case. Then we find h from (21), (29) and (30):

$$h = \frac{A_0 p_0^{1/\gamma} u_0 B}{[p_0 + Bx(i_0 + \tfrac{1}{2}cx)]^{1/\gamma} V}. \tag{31}$$

Finally, the net power is calculated to be

$$P = \frac{A_0 p_0^{1/\gamma} u_0 \gamma}{\gamma - 1} \{[p_0 + BL(i_0 + \tfrac{1}{2}cL)]^{(\gamma-1/\gamma)} - p_0^{(\gamma-1/\gamma)}\}. \tag{32}$$

We find in this case, in contrast to our previous result, that the net power P depends on the applied magnetic field B. This situation occurs because the power per unit duct volume is Ei and E varies directly as B (see (10)) while i is assumed to be independent of B. In the previous case, i was inversely proportional to B (see (20)), so that the product Ei was independent of B.

Although the solution of the second case was quite simple, it should be pointed out that, in general, when i is one of the two variables specified, the equations will be difficult to solve. On the other hand, the first case was treated readily, and any other case in which we specify two of the four variables p, ρ, u and A will also be solved easily. Since these latter cases are those which would be of most interest for practical applications, the concept of isentropic one-dimensional MHD channel flows developed here should prove useful.

§ 4. *Conclusions.* In the preceding sections, we have formulated the one-dimensional approximation to isentropic MHD channel flow and have shown how solutions to the resulting equations may be obtained. These solutions can be interpreted as describing either a crossed-field accelerator or generator depending on whether the net power P is negative or positive. For example, if in the first case considered in the last section, where velocity increases linearly with x, we select our constants such that P is negative (power added to gas), then this is an example of a useful crossed-field accelerator. If P were positive, the device would be a generator of rather unlikely design. The second case could, on the other hand, be considered a generator (since velocity is constant) by taking i_0 to be some negative value and limiting the duct length L to a value less than the length at which the current density i is reduced to zero.

In either application, the present approximation will be valuable for the description of high efficiency devices.

Received 19th September, 1960.

REFERENCES

1) Rosa, R. J., and A. Kantrowitz, Avco Research Laboratory, February 1960.
2) Podolsky, B. and G. L. Borman, Plasma Acceleration, edited by S. W. Kash, Stanford Univ. Press, Stanford, California, 1960.
3) Resler, E. L., Jr. and W. R. Sears, J. Aero. Sci. **25** (1959) 235.
4) McCune, J. E. and W. R. Sears, J. Aero. Sci. **27** (1960) 139.

MARTINUS NIJHOFF — PUBLISHER — THE HAGUE

MICROPROJECTION WITH X-RAYS

by

ONG SING POEN

TECHNOLOGICAL UNIVERSITY, DELFT

One of the 5 types of X-ray microscopes is the projection microscope, originally proposed by Von Ardenne in 1939 and realized by Cosslett and Nixon in 1951.
With the aid of an ultra-fine-focus X-ray tube with a spot diameter of 1–0.1 micron, an enlarged X-ray shadow image is projected on a screen or film. Due to negligible scattering and refraction clear absorption images can be obtained. A special feature is the great depth of focus. Thus ideal stereo images can be made, showing the three dimensional mass absorption distribution of the specimen. This will be of great importance for both research (medical, biological, metallurgical, criminological, etc.) and technology (rubber-, textile-, paper-industry etc.). In "Microprojecton with X-rays" the author describes his experiences in constructing and applying the projection microscope in practice, covering five years of research in this field. His book will serve as a guide to those who are intending to explore the possibilities of this type of microscope.

1959. 132 pages on art paper. With 42 figures and 38 illustrations.
Guilders 12.50

Obtainable through any bookseller or from the publisher